

Dark matter in (partially) composite Higgs models

Tommi Alanne^a Diogo Buarque Franzosi^b Mads T. Frandsen^c Martin Rosenlyst^c

^a*Max-Planck-Institut für Kernphysik, Saupfercheckweg 1, 69117 Heidelberg, Germany*

^b*Institut für Theoretische Physik, Universität Göttingen, Friedrich-Hund-Platz 1, 37077 Göttingen, Germany*

^c*CP³-Origins, University of Southern Denmark, Campusvej 55, DK-5230 Odense M, Denmark*

E-mail: tommi.alanne@mpi-hd.mpg.de, dbuarqu@gwdg.de,
frandsen@cp3.sdu.dk, rosenlyst@cp3.sdu.dk

ABSTRACT: We construct composite and partially composite Higgs models with complex pseudo-Nambu–Goldstone (pNGB) dark matter states from four-dimensional gauge-Yukawa theories with strongly interacting fermions. The fermions are partially gauged under the electroweak symmetry, and the dynamical electroweak symmetry breaking sector is minimal.

The pNGB dark matter particle is stable due to a U(1) technibaryon-like symmetry, also present in the technicolor limit of the models. However, the relic density is particle anti-particle symmetric and due to thermal freeze-out as opposed to the technicolor limit where it is typically due to an asymmetry.

The pNGB Higgs is composite or partially composite depending on the origin of the Standard Model fermion masses, which impacts the dark matter phenomenology. We illustrate the important features with a model example invariant under an $SU(4) \times SU(2) \times U(1)$ global symmetry.

Preprint: CP³-Origins-2018-031 DNR90

Contents

1	Introduction	2
2	The Model and the effective description	3
2.1	The condensates and electroweak embedding	4
2.2	Interactions between the \mathcal{R}_1 and \mathcal{R}_2 sectors	6
2.3	SM-fermion masses and vacuum alignment	7
3	Dark Matter	11
3.1	Annihilation cross sections	11
3.2	Experimental searches	16
4	Conclusions	19
A	Φ-interactions	20
B	Abelian bosons	20

1 Introduction

Gauge and gauge-Yukawa theories with strongly interacting fermion sectors at, or above, the weak scale underly several model frameworks for dynamical electroweak symmetry breaking (EWSB). This includes technicolor (TC) [1–5] and bosonic technicolor (bTC) [6–11], partially composite Higgs (pCH) [12–16], and composite-Higgs (CH) models [17–21]. These models can be realized with the same underlying four-dimensional gauge theories with fermions via different vacuum alignments—and by adding scalars in the bTC and pCH cases.

In the TC limit the Higgs is an excitation of the vacuum [5, 6, 22], and analogously to QCD there can be a global U(1) technibaryon symmetry which allows for the lightest technibaryon to be an asymmetric dark matter (DM) candidate [23–28]. It must typically be particle anti-particle asymmetric because of large annihilation cross sections from the strong interactions at the weak scale, although symmetric candidates from thermal freeze-out [29] or the bosonic seesaw portal production mechanism in bTC [30] can occur. This U(1) symmetry is often anomalous under weak interactions such that Standard Model (SM) sphalerons may equilibrate baryon and technibaryon numbers [24] and address the origin of the ratio of visible to dark relic densities.

In the CH vacuum, the Higgs is realized as a pseudo-Nambu–Goldstone boson (pNGB) with properties which may be tuned close to the SM Higgs by external interactions. However, the U(1) technibaryon symmetry present in the TC limit is typically lost. Instead, DM candidates in CH models have typically been constructed and stabilized using Z_2 symmetries, and the models are typically studied using purely an effective Lagrangian [31–35]. CH models with a preserved U(1) symmetry have also been considered; see e.g. Refs [36, 37], and at the level of an effective description Ref. [38] and with strongly interacting scalars [39].

Here we are interested in models with explicit four-dimensional descriptions in terms of elementary degrees of freedom that retain particles charged under a global U(1) symmetry in the CH vacuum. In particular, we are interested in models where the DM candidate charged under this stabilizing U(1) symmetry is a pNGB related to the dynamical symmetry breaking. This is simply realized with models where only part of the fermions are gauged under the electroweak (EW) interactions for which TC limits have been studied in e.g. Refs [26, 28, 40, 41]. We, therefore, consider models with $N_1 + N_2$ Weyl fermions transforming in representations \mathcal{R}_1 and \mathcal{R}_2 , respectively, of a new strongly interacting gauge group G_{TC} . Only the \mathcal{R}_1 fermions are gauged under the SM EW gauge group and responsible for EWSB. For fermion partial compositeness we comment on adding a third sector of N_3 QCD charged fermions in order to accommodate top partners.

The \mathcal{R}_2 sector was motivated both by achieving near-conformal dynamics [26, 40, 41] and by allowing for light asymmetric DM [28] in the TC limit. When aligning the \mathcal{R}_1 sector into the CH regime, the \mathcal{R}_2 sector can retain a U(1)-technibaryon-like symmetry, and thereby a composite DM candidate which, however, must now have a particle anti-particle symmetric relic density.

The simple model we study has $G_{\text{TC}} = \text{SU}(2)$, $N_1 = 4$ with \mathcal{R}_1 being the fundamental representation, and $N_2 = 2$ with \mathcal{R}_2 being the adjoint representation. The TC limit of this model was studied in Ref. [26], while Ref. [41] considered $\mathcal{R}_2 = \mathcal{R}_1$ with both inert and electroweak gauged fermions in the fundamental representation. The CH and pCH regimes of the \mathcal{R}_1 sector only were studied in Refs [21, 42] and [13–16], respectively. Since the model is formulated explicitly in terms of elementary constituents, the composite contributions to the spectrum may be predicted using lattice simulations. The \mathcal{R}_1 sector has recently been studied in e.g. Refs [43–45] and recent lattice studies have begun investigating models with multiple fermion representations [46, 47] and composite DM candidates [48–51].

The paper is organised as follows: In Sec. 2 we introduce the model framework, the

Table 1: The new fermion content and their representations under the gauge groups, as in [26].

	SU(2) _{TC}	SU(2) _W	U(1) _Y
(U_L, D_L)	\square	\square	0
\tilde{U}_L	\square	1	-1/2
\tilde{D}_L	\square	1	+1/2
λ_L	Adj	1	0
$\tilde{\lambda}_L$	Adj	1	0

model example with $SU(4) \times SU(2) \times U(1)$ symmetry and the effective description. In Sec. 3 we discuss the phenomenology of the DM candidate, the pNGB of the \mathcal{R}_2 sector, and the interplay with different possible origins of the SM-fermion masses. Finally, in Sec. 4 we give our conclusions.

2 The Model and the effective description

The model framework we propose consist of a new strongly interacting gauge group G_{TC} with N_1 Weyl fermions in the representation \mathcal{R}_1 and N_2 Weyl fermions in the representation \mathcal{R}_2 . The \mathcal{R}_1 fermions are gauged under the EW interactions, while the \mathcal{R}_2 fermions are inert. We also add interactions to provide SM-fermion masses and to align the vacuum into the CH regime. We will briefly discuss elementary scalars [6] and four-fermion operators of both the extended-TC (ETC) [1, 2] and fermion-partial-compositeness (PC) type [52] as examples of such interactions. In the latter case, we add a third sector with QCD charged fermions to accomodate a top partner, to be discussed in more detail in Sec. 2.3(iii).

In the minimal model example which we will study, the gauge group is chosen to be $G_{TC} = SU(2)_{TC}$ with \mathcal{R}_1 the fundamental representation and $N_1 = 4$. We further take \mathcal{R}_2 to be the adjoint representation and $N_2 = 2$ as in Ref. [26]. The fermion content in terms of left-handed Weyl fields, with $\tilde{\psi}_L \equiv \epsilon\psi_R^*$, along with their EW quantum numbers is presented in Table 1. The strongly interacting fermion sector features the global symmetry $SU(4) \times SU(2) \times U(1)$ at the quantum level. The spinors $Q = (U_L, D_L, \tilde{U}_L, \tilde{D}_L)$ and $\Lambda = (\lambda_L, \tilde{\lambda}_L)$ transform in the fundamental representations of the $SU(4)$ and $SU(2)$ subgroups of the global symmetry, respectively, where we drop a L subscript on Q and Λ for simplicity. The anomaly free ¹ U(1) acts on both fermion sectors as

$$Q \rightarrow e^{-i\alpha} Q, \quad \Lambda \rightarrow e^{i\frac{\alpha}{2}} \Lambda. \quad (2.1)$$

In the case of PC, where we need a larger gauge group, this charge assignment is different, and we will discuss this issue in Section 2.3.

The underlying fermionic Lagrangian we consider is

$$\mathcal{L}_{UV} = \bar{Q}i\not{D}Q + \bar{\Lambda}i\not{D}\Lambda + \delta\mathcal{L}_m + \delta\mathcal{L}, \quad (2.2)$$

¹The U(1) charges of Q and Λ make the corresponding current anomaly free since $(-1)4\text{Tr}[\tau^a \tau^b] + (1/2)2\text{Tr}[\epsilon^{acd}\epsilon^{bcd}] = 0$.

where $\delta\mathcal{L}$ are additional interactions including those responsible for vacuum alignment and SM-fermion masses, and we have collected the explicit mass terms for Q, Λ in $\delta\mathcal{L}_m$ with

$$\delta\mathcal{L}_m = \frac{1}{2}Q^T M_Q Q + \frac{1}{2}\Lambda^T M_\Lambda \Lambda + \text{h.c.}, \quad M_Q = \begin{pmatrix} m_1\epsilon & 0 \\ 0 & -m_2\epsilon \end{pmatrix}, \quad M_\Lambda = \begin{pmatrix} 0 & m \\ m & 0 \end{pmatrix}. \quad (2.3)$$

The mass terms preserve the subgroups $\text{Sp}(4) \in \text{SU}(4)$ and $U(1)_\Lambda \times Z_2 \subset \text{SU}(2) \times \text{U}(1)$. The EW gauging of the kinetic term of Q preserves the subgroup $\text{SU}(2)_W \times \text{U}(1)_Y \times \text{U}(1)_{\text{TB}} \subset \text{SU}(4)$ and the full $\text{SU}(2) \times \text{U}(1)$ part of the global symmetry.

2.1 The condensates and electroweak embedding

The dynamical condensates of the theory are

$$\langle Q_{\alpha,c}^I Q_{\beta,c'}^J \epsilon^{\alpha\beta} \epsilon^{cc'} \rangle \sim f^3 E_Q^{IJ}, \quad \langle \lambda_{\alpha,k}^A \lambda_{\beta,k'}^B \epsilon^{\alpha\beta} \delta^{kk'} \rangle \sim f_\Lambda^3 E_\Lambda^{AB} \quad (2.4)$$

with I, J and A, B flavor indices in the two sectors while α, β are spin and c, k are gauge indices. We expect the Goldstone boson decay constants f, f_Λ to be of the same order [26, 28] and will for simplicity take them to be identical later. The condensates break the global symmetries $\text{SU}(4)$ to $\text{Sp}(4)$ and $\text{SU}(2) \times \text{U}(1)$ to $U(1)_\Lambda \times Z_2$. The orientation of the condensate E_Q relative to the EW embedding determines whether we are in the TC limit or in the CH regime, and the orientation is in turn determined by the interactions in $\delta\mathcal{L}, \delta\mathcal{L}_m$. In the TC limit the $\text{Sp}(4)$ is aligned such that it only contains the $U(1)_{\text{EM}}$ subgroup of the electroweak symmetry group.

To describe the general vacuum alignment in the effective Lagrangian we identify an $\text{SU}(2)_L \times \text{SU}(2)_R$ subgroup in $\text{SU}(4)$ by the left and right generators

$$T_L^i = \frac{1}{2} \begin{pmatrix} \sigma_i & 0 \\ 0 & 0 \end{pmatrix}, \quad T_R^i = \frac{1}{2} \begin{pmatrix} 0 & 0 \\ 0 & -\sigma_i^T \end{pmatrix}, \quad (2.5)$$

where σ_i are the Pauli matrices. The EW subgroup is gauged after identifying the generator of hypercharge with T_R^3 ; see, e.g., Refs [18, 21, 53] for details.

The alignment between the EW subgroup and the stability group $\text{Sp}(4)$ can then be conveniently parameterized by an angle, θ , after identifying the vacua that leave the EW symmetry intact, E_Q^\pm , and the one breaking it completely to $U(1)_{\text{EM}}$ of electromagnetism, E_Q^B , with:

$$E_Q^\pm = \begin{pmatrix} i\sigma_2 & 0 \\ 0 & \pm i\sigma_2 \end{pmatrix}, \quad E_Q^B = \begin{pmatrix} 0 & 1 \\ -1 & 0 \end{pmatrix}, \quad E_\Lambda = \begin{pmatrix} 0 & 1 \\ 1 & 0 \end{pmatrix} \quad (2.6)$$

where we have also written the Λ -sector vacuum matrix, E_Λ . The true $\text{SU}(4)$ vacuum can be written as a linear combination of the EW-preserving and EW-breaking vacua, $E_Q = c_\theta E_Q^- + s_\theta E_Q^B$. We use the short-hand notations $s_x \equiv \sin x$, $c_x \equiv \cos x$, and $t_x \equiv \tan x$ throughout. Either choice of E_Q^\pm is equivalent [54], and here we have chosen E_Q^- . The vacuum alignment of the Λ -sector, described by the matrix E_Λ , is kept fixed, independent of the angle, θ .

In the CH vacuum with $0 < \theta < \pi/2$ the unbroken global symmetry group is reduced from $\text{Sp}(4)$ to $U(1)_{\text{EM}} \times U(1)_\Lambda \times Z_2$ after gauging. In the limit $\theta = \pi/2$ referred to as the TC vacuum the unbroken symmetry group is $U(1)_{\text{EM}} \times U(1)_{\text{TB}} \times U(1)_\Lambda \times Z_2$. In the EW unbroken vacuum with $\theta = 0$ it is $\text{SU}(2)_W \times \text{U}(1)_Y \times U(1)_\Lambda \times Z_2$.

The Goldstone excitations around the vacuum are then parameterized by

$$\begin{aligned} \Sigma_Q &= \exp \left[2\sqrt{2}i \left(\frac{\Pi_Q}{f} - \frac{1}{3} \frac{\Theta}{f_\Theta} \mathbb{1}_4 \right) \right] E_Q, \\ \Sigma_\Lambda &= \exp \left[2\sqrt{2}i \left(\frac{\Pi_\Lambda}{f_\Lambda} + \frac{1}{6} \frac{\Theta}{f_\Theta} \mathbb{1}_2 \right) \right] E_\Lambda, \end{aligned} \quad (2.7)$$

with

$$\Pi_Q = \sum_{i=1}^5 \Pi_Q^i X_Q^i, \quad \Pi_\Lambda = \sum_{i=1}^2 \Pi_\Lambda^i X_\Lambda^i, \quad (2.8)$$

where $X_{Q,\Lambda}$ are the θ -dependent broken generators of SU(4) and SU(2) and can be found explicitly in Refs [26, 54]. The Θ state is the only state connecting the two sectors at the level of single trace terms in the effective Lagrangian and its U(1) charges under each sector follow from Eq. (2.1).

For simplicity, we will henceforth use the notations $h \equiv \Pi_Q^4$ and $\eta \equiv \Pi_Q^5$ for the composite Higgs, and the CP-odd pNGB of the Q sector, resp., and $\Phi \equiv \frac{1}{\sqrt{2}}(\Pi_\Lambda^1 - i\Pi_\Lambda^2)$, $\bar{\Phi} \equiv \frac{1}{\sqrt{2}}(\Pi_\Lambda^1 + i\Pi_\Lambda^2)$ for the Λ -sector pNGBs, corresponding to $\Lambda^T C \Lambda$ and $\bar{\Lambda} C \bar{\Lambda}^T$ states.

The states in the EW unbroken limit with $s_\theta = 0$ (upper) and TC vacuum with $s_\theta = 1$ (lower) are given in Table 2. In the composite Higgs range the states correspond to those in the EW unbroken vacuum except $h \equiv \Pi_Q^4 \sim c_\theta(\bar{U}U + \bar{D}D) + s_\theta \text{Re} U^T C D$, see e.g. Ref. [53].

Table 2: Table of pNGB states in the EW unbroken limit with $s_\theta = 0$ (upper) and the TC limit $s_\theta = 1$ (lower)

	U(1) _{TB}	U(1) _Λ	Z ₂
$h \equiv \Pi_Q^4 \sim \bar{U}U + \bar{D}D$	–	0	0
$\eta \equiv \Pi_Q^5 \sim \text{Im} U^T C D$	–	0	0
$\Phi \equiv (\Pi_\Lambda^1 - i\Pi_\Lambda^2)/\sqrt{2} \sim \Lambda^T C \Lambda$	–	1	0
$\bar{\Phi} \equiv (\Pi_\Lambda^1 + i\Pi_\Lambda^2)/\sqrt{2} \sim \bar{\Lambda} C \bar{\Lambda}^T$	–	–1	0
$\Theta \sim i(\bar{U}\gamma^5 U + \bar{D}\gamma^5 D - (1/2)\bar{\Lambda}\gamma^5 \Lambda)$	–	0	0
$\Pi_{UD} \equiv (\Pi_Q^4 - i\Pi_Q^5)/\sqrt{2} \sim U^T C D$	$\frac{1}{\sqrt{2}}$	0	0
$\Pi_{\bar{U}\bar{D}} \equiv (\Pi_Q^4 + i\Pi_Q^5)/\sqrt{2} \sim \bar{U} C \bar{D}^T$	$-\frac{1}{\sqrt{2}}$	0	0
Φ	0	1	0
$\bar{\Phi}$	0	–1	0
Θ	0	0	0

Below the condensation scale, the Lagrangian of Eq. (2.2), gauged under the EW interactions, yields

$$\mathcal{L}_{\text{eff}} = \mathcal{L}_{\text{kin}} - V_{\text{eff}}, \quad (2.9)$$

where the kinetic terms are

$$\mathcal{L}_{\text{kin}} = \frac{f^2}{8} \text{Tr}[D_\mu \Sigma_Q^\dagger D^\mu \Sigma_Q] + \frac{f_\Lambda^2}{8} \text{Tr}[\partial_\mu \Sigma_\Lambda^\dagger \partial^\mu \Sigma_\Lambda], \quad (2.10)$$

with

$$D_\mu \Sigma_Q = \partial_\mu \Sigma_Q - i(G_\mu \Sigma_Q + \Sigma_Q G_\mu^T), \quad (2.11)$$

and the EW gauge fields are encoded in the covariant derivative

$$G_\mu = gW_\mu^i T_L^i + g'B_\mu T_R^3. \quad (2.12)$$

The kinetic term of Θ is canonically normalized only if $f_\Theta = f = f_\Lambda$ which we will assume for simplicity. In the general case, the kinetic terms must be renormalized but based on Casimir scaling we expect them to be of the same size [26, 28].

The EW gauge interactions contribute to the effective potential at the one-loop level, but the contribution is higher order as compared to the vector-like mass terms in Eq. (2.3), and numerically subleading due to the smallness of the EW gauge couplings as compared to the top-loop contributions arising from the four-fermion interactions. We discuss the latter below.

The effective potential, at the lowest order, is given by

$$V_{\text{eff},m}^0 = 2\pi c_Q f^3 \text{Tr} \left[M_Q \Sigma_Q^\dagger + \Sigma_Q M_Q^\dagger \right] + 2\pi c_\Lambda f_\Lambda^3 \text{Tr} [M_\Lambda \Sigma_\Lambda^\dagger + \Sigma_\Lambda M_\Lambda^\dagger], \quad (2.13)$$

where c_Q, c_Λ are non-perturbative $\mathcal{O}(1)$ constants, and we use the numerical value $c_Q \approx 1.5$ suggested by the lattice simulations [43]. The mass terms involving M_Q (as well as the subleading EW gauge interactions) prefer the vacuum where the EW is unbroken as we discuss below. The correct vacuum alignment must therefore be ensured by the SM-fermion mass generation mechanism.

2.2 Interactions between the \mathcal{R}_1 and \mathcal{R}_2 sectors

From the single trace terms in Eq. (2.13), the only interactions between the \mathcal{R}_1 and \mathcal{R}_2 sectors are those involving the Θ state. At the next leading order all interactions between the \mathcal{R}_1 and \mathcal{R}_2 sectors arise from double trace terms

$$\begin{aligned} \mathcal{L}_{Q,\Lambda} = & \frac{c_1}{4\pi} \text{Tr} [D_\mu \Sigma_Q^\dagger D^\mu \Sigma_Q] \text{Tr} [\partial_\mu \Sigma_\Lambda^\dagger \partial^\mu \Sigma_\Lambda] \\ & - \frac{c_2}{4\pi} f_\Lambda \text{Tr} [D_\mu \Sigma_Q^\dagger D^\mu \Sigma_Q] \text{Tr} [M_\Lambda \Sigma_\Lambda^\dagger + \Sigma_\Lambda M_\Lambda^\dagger - 2M_\Lambda E_\Lambda] \\ & - \frac{c_3}{4\pi} f_\Lambda f \text{Tr} [M_Q \Sigma_Q^\dagger + \Sigma_Q M_Q^\dagger + 2M_Q E_Q] \text{Tr} [M_\Lambda \Sigma_\Lambda^\dagger + \Sigma_\Lambda M_\Lambda^\dagger - 2M_\Lambda E_\Lambda] \\ & - \frac{c_4}{4\pi} f \text{Tr} [M_Q \Sigma_Q^\dagger + \Sigma_Q M_Q^\dagger + 2M_Q E_Q] \text{Tr} [\partial_\mu \Sigma_\Lambda^\dagger \partial^\mu \Sigma_\Lambda] + \dots, \end{aligned} \quad (2.14)$$

where $c_i, i = 1, \dots, 4$ are the Gasser–Leutwyler type coefficients [55], and $c_i \sim \mathcal{O}(1)$ by naive dimensional analysis in analogy with QCD [56]. We have for simplicity shifted the c_2 and c_3 terms such that Φ, h , and the EW gauge boson masses and kinetic terms do not acquire additional contributions from these higher-order terms, but are instead determined by Eqs (2.13), (2.24), and (2.10), resp.

Expanding Eqs (2.13) and (2.14) yields

$$\begin{aligned} \mathcal{L}_{Q,\Lambda} \supset & \frac{m_\Phi^2}{f_\Lambda^2} \Phi \bar{\Phi} \left(g_h h + \frac{1}{2} g_{ZZ} Z_\mu Z^\mu + g_{WW} W_\mu^+ W^{-\mu} + \frac{1}{2} g_{\Theta\Theta} \Theta^2 + \frac{1}{2} g_{hh} h^2 + \frac{1}{2} g_{\eta\eta} \eta^2 \right. \\ & \left. + \frac{1}{2} g_{\partial\Theta} \partial_\mu \Theta \partial^\mu \Theta + \frac{1}{2} g_{\partial h} \partial_\mu h \partial^\mu h + \frac{1}{2} g_{\partial\eta} \partial_\mu \eta \partial^\mu \eta \right) \\ & + \frac{1}{f_\Lambda^2} \partial_\mu \Phi \partial^\mu \bar{\Phi} \left(d_h h + \frac{1}{2} d_{ZZ} Z_\mu Z^\mu + d_{WW} W_\mu^+ W^{-\mu} + \frac{1}{2} d_{hh} h^2 + \frac{1}{2} d_{\eta\eta} \eta^2 \right. \\ & \left. + \frac{1}{2} d_{\partial\Theta} \partial_\mu \Theta \partial^\mu \Theta + \frac{1}{2} d_{\partial h} \partial_\mu h \partial^\mu h + \frac{1}{2} d_{\partial\eta} \partial_\mu \eta \partial^\mu \eta \right), \end{aligned} \quad (2.15)$$

where

$$m_\Phi^2 = -16\pi c_\Lambda f_\Lambda m, \quad (2.16)$$

analogously to the Gell-Mann–Oakes–Renner relation in QCD [57]. The mass appears as a common prefactor of all non-derivative terms as a consequence of the Goldstone nature of Φ . The couplings involving the Θ state $g_{\Theta\Theta}$ and $g_{\partial\Theta}$ are the only ones not arising from a double trace term. We give the explicit couplings in appendix A.

Besides the anomaly-free Θ state, a Θ' state corresponding to the U(1) which is quantum anomalous is also present in the spectrum of the theory and can mix with Θ . Its mass is generated by instanton effects related to the U(1) anomaly [58]. We provide more details in App. B. We assume for simplicity that Θ' mass is large and it decouples.

The anomaly-free state Θ on the other hand receive its mass from explicit U(1) breaking terms, like the vector-like mass terms of Eq. (2.13), which also generate interactions between Θ and other pNGBs. Explicitly, the relevant terms (excluding derivatives) up to quartic order are given by

$$\begin{aligned} \mathcal{L} \supset & \frac{8\pi}{9f_\Theta^2} (4c_Q f^3 m_Q c_\theta + c_\Lambda f_\Lambda^3 m) \Theta^2 - \frac{16\sqrt{2}\pi}{3f_\Theta} c_Q f^2 (m_1 - m_2) \Theta \eta \\ & - \frac{4}{9\pi f_\Theta^2} s_\theta m_Q (8\pi^2 c_Q f^2 + c_3 f_\Lambda m) h \Theta^2 - \frac{32m}{9\pi f_\Theta^2 f_\Lambda} (2\pi^2 c_\Lambda f_\Lambda^2 + c_3 m_Q f c_\theta) \Theta^2 \Phi \bar{\Phi} \\ & + \frac{2}{9\pi f f_\Theta^2} \left\{ (h^2 + \eta^2) \left[4\sqrt{2}\pi^2 c_Q f f_\Theta (m_1 - m_2) \Theta \eta - c_\theta m_Q (8\pi^2 c_Q f^2 + c_3 m f_\Lambda) \Theta^2 \right] \right. \\ & \quad \left. + \frac{4\sqrt{2}}{9f_\Theta} (m_1 - m_2) (8\pi^2 c_Q f^2 + 3c_3 m f_\Lambda) \Theta^3 \eta \right\} \end{aligned} \quad (2.17)$$

where $m_Q \equiv m_1 + m_2$. We also assume that $m_1 = m_2$ so mass mixing is absent in the pseudoscalar sector.

The relevance of the Θ state and its interactions for our study is that the quartic term $\Phi \bar{\Phi} \Theta^2$ can erase the thermal relic density of Φ unless $m_\Theta > m_\Phi$ or $m \ll f_\Lambda$. In the following we require $m_\Theta > m_\Phi$ and this imposes non-trivial constraints on the parameter space.

2.3 SM-fermion masses and vacuum alignment

The composite sector must be extended to provide SM-fermion masses and correct vacuum alignment. Here we briefly comment on the three different possibilities which will impact the DM phenomenology. Further ways to distinguish these possibilities using the pseudoscalars analogous to the QCD η, η' states have been discussed in Ref. [59].

(i) ETC-type four-fermion operators. One possibility is to add four-fermion operators as in Ref. [17]. Such four-fermion operators could themselves arise from the exchange of heavy scalar multiplets but also from heavy vectors as in ETC [2].

Explicitly for the top quark, after integrating out heavy states, we would have

$$\mathcal{L}_{4f} \sim - \frac{Y_t Y_U}{\Lambda_t^2} (\bar{q}_L t_R)_\alpha^\dagger (Q^T P_\alpha Q) + \text{h.c.}, \quad (2.18)$$

where the spurion, P_α , projects out the EW components such that $Q^T P_\alpha Q$ transforms as EW doublet with hypercharge +1/2. Upon the condensation of the techniquarks, this yields a contribution to the top mass, i.e.

$$\mathcal{L}_{4f} \sim -4\pi c_Q f^3 \frac{Y_t Y_U}{\Lambda_t^2} \text{Tr}[P_1 \Sigma] \bar{t} t = -y'_t f s_\theta \bar{t} t - y'_t c_\theta h \bar{t} t + \dots, \quad (2.19)$$

where

$$y'_t \equiv \frac{4\pi c_Q f^2 Y_t Y_U}{\Lambda_t^2} = \frac{m_t}{v_w}. \quad (2.20)$$

This yields the Higgs-top coupling

$$y_{h\bar{t}t} = y'_t c_\theta = \frac{m_t}{v_w} c_\theta, \quad (2.21)$$

and gives a contribution to the effective potential via the top loop:

$$V_{\text{top}} = -C_t y_t'^2 f^4 \sum_\alpha |\text{Tr}[P_\alpha \Sigma_Q]|^2 = -C_t y_t'^2 f^4 s_\theta^2 + \dots, \quad (2.22)$$

where C_t encodes the non-perturbative top-loop effects. The vacuum alignment is dominantly given by balancing the top contribution and contribution from the explicit techniquark mass terms [21]:

$$c_\theta = -\frac{4\pi c_Q m_Q}{C_t y_t'^2 f}. \quad (2.23)$$

The Higgs mass is given by

$$m_h^2 = -2f (4\pi c_Q m_Q c_\theta + C_t y_t'^2 f c_{2\theta}) = 2C_t y_t'^2 f^2 s_\theta^2 = 2C_t m_t^2. \quad (2.24)$$

Thus the correct Higgs mass is reproduced for $C_t \sim \frac{1}{4}$. Furthermore, the mass of η reads

$$m_\eta^2 = m_h^2 / s_\theta^2. \quad (2.25)$$

We can write the mass of Θ from Eq. (2.17) now as

$$m_\Theta^2 = \frac{8}{9} m_\eta^2 c_\theta^2 + \frac{1}{9} m_\Phi^2. \quad (2.26)$$

Requiring that $m_\Theta > m_\Phi$ leads to the constraint

$$m_\Phi < m_\eta c_\theta, \quad (2.27)$$

and further after parametrizing $m_\Phi = \epsilon f$, to a relation between s_θ and ϵ :

$$\epsilon^2 < \frac{m_h^2}{v_w^2} (1 - s_\theta^2) \approx \frac{1}{4} (1 - s_\theta^2). \quad (2.28)$$

(ii) Partially composite Higgs. Alternatively we may add a multiplet of elementary scalars containing at least an $\text{SU}(2)_W$ doublet with Yukawa couplings to SM fermions as in Refs [6, 12–14, 16]. We will focus on the simplest example with H an $\text{SU}(2)_W$ doublet by adding to the UV Lagrangian above the interactions:

$$\begin{aligned} \mathcal{L}_H = & D_\mu H^\dagger D^\mu H - m_H^2 H^\dagger H - \lambda_H (H^\dagger H)^2 \\ & - y_U H_\alpha (Q^T P_\alpha Q) - y_D \tilde{H}_\alpha (Q^T \tilde{P}_\alpha Q) + \text{h.c.}, \end{aligned} \quad (2.29)$$

where the elementary Higgs doublet is given by

$$H_\alpha = \frac{1}{\sqrt{2}} \begin{pmatrix} \sigma_h - i\pi_h^3 \\ -(\pi_h^2 + i\pi_h^1) \end{pmatrix}, \quad (2.30)$$

where $\tilde{H} = \epsilon H^*$. The antisymmetric contractions are kept implicit.

The above Yukawa interactions induce the following lowest-order operators to the effective potential:

$$V_{\text{pCH}} = 4\pi c_Q f^3 \left(y_U H_\alpha \text{Tr}[P_\alpha \Sigma_Q] + y_D \tilde{H}_\alpha \text{Tr}[\tilde{P}_\alpha \Sigma_Q] + \text{h.c.} \right). \quad (2.31)$$

This part of the potential prefers the TC vacuum such that the final vacuum alignment in this case is given by

$$t_\theta = -\frac{(y_U + y_D)v}{\sqrt{2}(m_1 + m_2)} = -\frac{v y_Q}{\sqrt{2} m_Q}, \quad (2.32)$$

where $v \equiv \langle \sigma_h \rangle$, $y_Q \equiv y_U + y_D$ and again $m_Q = m_1 + m_2$.

The two CP-even mass eigenstates in this partially composite Higgs case are given in terms of the interaction eigenstates by [16]

$$h_1 = c_\alpha \sigma_h - s_\alpha h, \quad h_2 = s_\alpha \sigma_h + c_\alpha h, \quad (2.33)$$

where as above we have first identified $h \equiv \Pi^4$, and the angle, α , is determined by

$$t_{2\alpha} = \frac{f v s_{2\theta}}{(1 + \delta) f^2 s_\theta^2 - v^2}, \quad \text{where} \quad \delta \equiv \frac{2\lambda_H v^2}{m_H^2 + \lambda_H v^2}. \quad (2.34)$$

The ordinary CH case corresponds to $s_\alpha = -1$, $h_1 = h$. In this case, the η mass is given by

$$m_\eta^2 = \frac{m_h^2 t_\alpha}{t_\alpha + c_\theta / t_\beta}, \quad (2.35)$$

where the angle β is defined by

$$t_\beta = \frac{v}{f s_\theta}. \quad (2.36)$$

The mass of Θ can now be written as

$$m_\Theta^2 = \frac{8}{9} m_\eta^2 + \frac{1}{9} m_\Phi^2. \quad (2.37)$$

Requiring that $m_\Theta > m_\Phi = \epsilon f$ leads again to a condition between s_θ and ϵ :

$$\epsilon^2 < \frac{m_\eta^2}{v_w^2} s_\theta^2. \quad (2.38)$$

(iii) Fermion partial compositeness. Finally in the partial compositeness scenario we add baryon-like operators as in Ref. [52]. In this case the underlying theory has to be extended with extra QCD charged fermions in order to construct the top partners and to enlarge the G_{TC} gauge group to ensure asymptotic freedom as studied in e.g. Ref. [19]. The effect of the partial compositeness operators into vacuum alignment was extensively discussed in Ref. [60]. The vacuum alignment phenomenology depends on in which representation of the global symmetry group the top partners are embedded. For concreteness, we will consider the top partners in the symmetric representation of $\text{SU}(4)$.

The top mass and linear couplings to pNGBs can be written as [60]

$$\begin{aligned} & \frac{C_{yS}}{4\pi} y_{t_L} y_{t_R} f (Q_1 t^c)^\dagger \text{Tr}[P_Q^1 \Sigma^\dagger P_t \Sigma^\dagger] + \text{h.c.} \\ & = (Q_1 t^c)^\dagger \left(m_{\text{top}} + \frac{m_{\text{top}}}{v} \left(\frac{c_{2\theta}}{c_\theta} h - i \frac{s_\theta}{c_\theta} \eta \right) + \dots \right) + \text{h.c.}, \end{aligned} \quad (2.39)$$

with $C_{yS} \sim \mathcal{O}(1)$, $m_t = \frac{C_{yS}}{4\pi} y_{tL} y_{tR} c_\theta s_\theta f$, and the contribution to the effective potential is given by

$$\begin{aligned} V_{\text{PC}} &= \frac{C_{tS}}{(4\pi)^2} f^4 \left(y_{tL}^4 \text{Tr}[P_Q^\alpha \Sigma^\dagger P_Q^\beta \Sigma^\dagger] \text{Tr}[\Sigma P_{Q\alpha}^\dagger \Sigma P_{Q\beta}^\dagger] \right. \\ &\quad + y_{tR}^4 \text{Tr}[P_t \Sigma^\dagger P_t \Sigma^\dagger] \text{Tr}[\Sigma P_t^\dagger \Sigma P_t^\dagger] \\ &\quad \left. + y_{tL}^2 y_{tR}^2 \text{Tr}[P_Q^\alpha \Sigma^\dagger P_t \Sigma^\dagger] \text{Tr}[\Sigma P_{Q\alpha}^\dagger \Sigma P_t^\dagger] \right) \\ &= \frac{C_{tS}}{(4\pi)^2} f^4 \left(y_{tL}^4 s_\theta^4 + y_{tR}^4 c_\theta^4 + y_{tL}^2 y_{tR}^2 c_\theta^2 s_\theta^2 \right), \end{aligned} \quad (2.40)$$

where

$$P_Q^1 = \frac{1}{\sqrt{2}} \begin{pmatrix} 0 & 0 & 1 & 0 \\ 0 & 0 & 0 & 0 \\ 1 & 0 & 0 & 0 \\ 0 & 0 & 0 & 0 \end{pmatrix}, \quad P_Q^2 = \frac{1}{\sqrt{2}} \begin{pmatrix} 0 & 0 & 0 & 0 \\ 0 & 0 & 1 & 0 \\ 0 & 1 & 0 & 0 \\ 0 & 0 & 0 & 0 \end{pmatrix}, \quad P_t = \frac{1}{\sqrt{2}} \begin{pmatrix} 0 & 0 & 0 & 0 \\ 0 & 0 & 0 & 0 \\ 0 & 0 & 0 & 1 \\ 0 & 0 & 1 & 0 \end{pmatrix}, \quad (2.41)$$

and $C_{tS} \sim \mathcal{O}(1)$.

Now the alignment condition reads

$$m_Q = \frac{4\pi C_{tS}}{c_Q C_{yS}^4 y_{tR}^4 f^3} \left[\frac{m_t^2}{c_\theta^3 s_\theta^2} \left(\frac{C_{yS}^2}{(4\pi)^2} y_{tR}^4 f^2 c_\theta^2 c_{2\theta} + 2m_t^2 \right) - 2 \frac{C_{yS}^4}{(4\pi)^4} y_{tR}^8 f^4 c_\theta^3 \right], \quad (2.42)$$

and the Higgs mass is given by

$$\begin{aligned} m_h^2 &= \frac{(4\pi)^2 C_{tS}}{C_{yS}^4 y_{tR}^4 f^2} \left[\frac{C_{yS}^2}{(4\pi)^2} f^2 y_{tR}^4 \left(\frac{3C_{yS}^2}{(4\pi)^2} y_{tR}^4 f^2 s_{2\theta}^2 + 2(t_\theta^2 - 5) m_t^2 \right) + m_t^4 (16/s_{2\theta}^2 - 2/c_\theta^4) \right] \\ &= \frac{32\pi^2 C_{tS}}{C_{yS}^4} \left(\frac{4m_t^4}{y_{tR}^4 v_w^2} - \frac{5C_{yS}^2}{(4\pi)^2} m_t^2 + \frac{6C_{yS}^4}{(4\pi)^4} y_{tR}^4 v_w^2 \right) + \mathcal{O}(s_\theta^2). \end{aligned} \quad (2.43)$$

Obtaining the correct Higgs mass, requires a small hierarchy $C_{tS} < C_{yS}$. Finally, the η mass can be written as

$$m_\eta^2 = \frac{4C_{tS}}{(4\pi)^2} f^2 y_{tR}^4 c_\theta^2 - \frac{8\pi^2 C_{tS} m_t^2}{C_{yS}^4 f^2 y_{tR}^4 s_\theta^2 c_\theta^4} \left(\frac{C_{yS}^2}{(4\pi)^2} f^2 y_{tR}^4 (c_{4\theta} + 2c_{2\theta} + 1) + 8m_t^2 \right). \quad (2.44)$$

One possible extension of our model to provide the top partners is to have four Weyl fermions, Q , in the fundamental (\mathbf{F}), another six, χ , in the two-index anti-symmetric, \mathbf{A}_2 , as detailed in Ref. [20], and keep the inert sector with λ -fermions still in the adjoint representation (\mathbf{G}) of G_{TC} . In this case, it is also necessary to modify the gauge group in order to ensure asymptotic freedom, one possibility being $G_{\text{TC}} = \text{Sp}(N_{\text{TC}})$. The enhanced global symmetry is then $\text{SU}(4)/\text{Sp}(4) \times \text{SU}(2)/\text{SO}(2) \times \text{SU}(6)/\text{SO}(6) \times \text{U}(1)^2$. Asymptotic freedom is guaranteed by $N_{\text{TC}} = 2 < 3$, where the first coefficient b of the beta function is positive[26, 61], i.e.

$$b = \frac{11}{3} C_2(\mathbf{G}) - \frac{2}{3} (4T(\mathbf{F}) + 2T(\mathbf{G}) + 6T(\mathbf{A}_2)) = -\frac{10}{3} (N_{\text{TC}} - 3) > 0 \quad (2.45)$$

with $T(\mathcal{R}) = 1, 2N_{\text{TC}} - 2, 2N_{\text{TC}} + 2$ the index of representation $\mathcal{R} = \mathbf{F}, \mathbf{A}_2, \mathbf{G}$ respectively. The two anomaly-free $\text{U}(1)$ give rise to two extra pNGBs. The Q, χ and λ charges under these $\text{U}(1)$ are defined by the anomaly cancellation

$$q_Q T(F) + q_\chi T(A_2) + q_\lambda T(G) = 0 \Rightarrow q_\lambda = -\frac{1}{3} q_Q - q_\chi. \quad (2.46)$$

The two states will mix but we leave a detailed study for the future and restrict to the simple case where the χ -sector (as well as the anomalous Θ') decouple (for instance with an explicit χ mass) so that the lightest Θ -state can be determined by the charge assignment $q_Q = -1$, $q_\lambda = 1/3$. All interactions of the Θ -sector then have to be modified accordingly; in particular the mass relation between Φ and Θ is modified to

$$m_\Theta^2 = \frac{1}{4q_Q^2 + 2q_\lambda} (4q_Q^2 m_\eta^2 c_\theta^2 + 2q_\lambda^2 m_\Phi^2) = \frac{1}{19} (18m_\eta^2 c_\theta^2 + m_\Phi^2). \quad (2.47)$$

Notice, however, that upon the requirement $m_\Theta > m_\Phi$, this leads to same constraint as in the ETC case, Eq. (2.27): $m_\Phi < m_\eta c_\theta$. A more general discussion allowing a small mass for χ is provided in App. B.

3 Dark Matter

Before studying the phenomenology of the DM state, Φ , it is illustrative to briefly discuss the relation between the TC and CH regimes. In the TC limit the Π_{UD} state in Table 2 is stable due to the $U(1)_{\text{TB}}$ symmetry which is only violated by the EW anomaly above the EW scale. The kinetic term in the Lagrangian in Eq. (2.10) includes contact interactions of Π_{UD} with the SM gauge bosons of the form

$$\mathcal{L}_{\text{kin}} \supset -\frac{g^2}{2} s_\theta^2 W_\mu^+ W^{-\nu} \Pi_{UD} \bar{\Pi}_{UD} \quad (3.1)$$

which lead to a large thermal cross section

$$\begin{aligned} \langle \sigma v \rangle &= \frac{g^4 s_\theta^4}{128\pi m_{\Pi_{UD}}^2} \sqrt{1 - \frac{m_W^2}{m_{\Pi_{UD}}^2}} \left(\frac{4m_{\Pi_{UD}}^4}{m_W^4} - \frac{4m_{\Pi_{UD}}^2}{m_W^2} + 3 \right) \\ &= \frac{g^4 s_\theta^4 m_{\Pi_{UD}}^2}{32\pi m_W^4} + \mathcal{O}(m_W^2/m_{\Pi_{UD}}^2) \\ &\simeq 2 \cdot 10^{-24} \text{ cm}^3/\text{s} \frac{s_\theta^4 m_{\Pi_{UD}}^2}{m_W^2} \end{aligned} \quad (3.2)$$

In the TC limit where $s_\theta = 1$, the Π_{UD} state can therefore only be thermal dark matter if its mass is just below the W mass threshold where the annihilation cross-section is kinematically suppressed [29]. For $m_{\Pi_{UD}} > m_W$ the annihilation cross section is too efficient such that Π_{UD} must instead be asymmetric if it is to be the DM as in [26, 29]. In the CH parameter regime, with say $s_\theta \lesssim 0.1$, the pNGB η , with a similar annihilation cross-section and with a weak scale mass, would be a WIMP candidate if it were stable but topological interactions make it unstable.

However the Φ state of the \mathcal{R}_2 sector in the extended models considered here remains protected by the $U(1)_\Lambda$ symmetry in both the TC and CH vacua. The contact interactions of Φ with the SM gauge bosons is not only suppressed by s_θ in the CH vacuum, but also by the fact that the interactions arise only from the double trace terms in Eq. (2.14).

In the following, we will compute the thermal annihilation cross sections for the three different cases for SM-fermion mass generation outlined in Sec. 2.3.

3.1 Annihilation cross sections

We list the dominant annihilation cross sections for different channels below. For simplicity, we write down explicitly here only the channels $\Phi\bar{\Phi} \rightarrow h_1 h_1, VV$. Notice that the condition

$m_\Theta > m_\Phi$ implies also $m_\eta > m_\Phi$ in all the cases of SM-fermion mass generation that we consider; see Eqs (2.26), (2.37), and (2.47). In the numerical analysis we keep all the interactions, and take into account the richer scalar sector in the pCH case including channels $\Phi\bar{\Phi} \rightarrow h_i h_j$, $i = 1, 2$.

$$\begin{aligned} \langle v\sigma \rangle_{h_1 h_1} = & \frac{1}{16\pi s f_\Lambda^4} \sqrt{1 - \frac{4m_{h_1}^2}{s}} \left[s_\alpha^2 m_\Phi^2 g_{hh} + s_\alpha^2 \frac{s - 2m_\Phi^2}{2} d_{hh} + s_\alpha^2 \frac{m_\Phi^2 (s - 2m_{h_1}^2)}{2} g_{\partial h} \right. \\ & + s_\alpha^2 \frac{s - 2m_\Phi^2}{2} \frac{s - 2m_{h_1}^2}{2} d_{\partial h} - s_\alpha \left(m_\Phi^2 g_h + \frac{s - 2m_\Phi^2}{2} d_h \right) \frac{g_{h_1 h_1 h_1}}{s - m_{h_1}^2} \\ & \left. + c_\alpha \left(m_\Phi^2 g_h + \frac{s - 2m_\Phi^2}{2} d_h \right) \frac{g_{h_2 h_1 h_1}}{s - m_{h_2}^2} \right]^2 + \mathcal{O}(c_i^3), \end{aligned} \quad (3.3)$$

and

$$\begin{aligned} \langle v\sigma \rangle_{VV} = & \frac{\delta_V}{8\pi s f_\Lambda^4} \sqrt{1 - \frac{4m_V^2}{s}} \left(3 + \frac{s(s - 4m_V^2)}{4m_V^4} \right) \left[m_\Phi^2 g_{VV} + \frac{s - 2m_\Phi^2}{2} d_{VV} \right. \\ & - s_\alpha \left(m_\Phi^2 g_h + \frac{s - 2m_\Phi^2}{2} d_h \right) \frac{g_{h_1 VV}}{s - m_{h_1}^2} \\ & \left. + c_\alpha \left(m_\Phi^2 g_h + \frac{s - 2m_\Phi^2}{2} d_h \right) \frac{g_{h_2 VV}}{s - m_{h_2}^2} \right]^2, \end{aligned} \quad (3.4)$$

for $V = W, Z$, and $\delta_{W,Z} = 1, \frac{1}{2}$, resp. The couplings g_i, d_i , $i = h, \partial h, hh, VV$ are given explicitly in appendix A, and the coupling $g_{h_1 h_1 h_1}, g_{h_1 VV}$, for CH and PC, and $g_{h_i h_1 h_1}, g_{h_i VV}$, $i = 1, 2$, for pCH case can be obtained from the Lagrangians given above. The CH and PC cases correspond to $s_\alpha = -1$, see Eq. (2.33).

Furthermore, the annihilation cross section $\Phi\bar{\Phi} \rightarrow t\bar{t}$ is given by

$$\begin{aligned} \langle v\sigma \rangle_{t\bar{t}} = & \frac{3}{4\pi s f_\Lambda^4} \sqrt{1 - \frac{4m_t^2}{s}} (s - 4m_t^2) \left[-s_\alpha \left(m_\Phi^2 g_h + \frac{s - 2m_\Phi^2}{2} d_h \right) \frac{g_{h_1 t\bar{t}}}{s - m_{h_1}^2} \right. \\ & \left. + c_\alpha \left(m_\Phi^2 g_h + \frac{s - 2m_\Phi^2}{2} d_h \right) \frac{g_{h_2 t\bar{t}}}{s - m_{h_2}^2} \right]^2, \end{aligned} \quad (3.5)$$

where $g_{h_{1,2} t\bar{t}}$ are the couplings of the mass eigenstates $h_{1,2}$ to the top quark, and again CH and PC cases correspond to $s_\alpha = -1$.

(i) ETC-type four-fermion operators. We consider first the annihilation cross section in the purely CH case with ETC-type SM-fermion masses, described in Sec. 2.3. The condition $m_\Theta > m_\Phi$ (cf. Eq. (2.26)) also implies $m_\eta > m_\Phi$, and therefore, the relevant annihilation channels are $\Phi\bar{\Phi} \rightarrow hh, VV, tt$.

Taking $m_\Phi = \epsilon f$, and $f_\Lambda = f = v_w/s_\theta$, and $m_Q = -\frac{m_h^2}{8\pi c_Q v_w t_\theta}$ fixed by the alignment condition Eq. (2.23), we find the leading- s_θ contribution to the annihilation cross section to be

$$\langle \sigma v \rangle_{hh, VV} = \frac{4s_\theta^2 \epsilon^2 [32\pi c_Q v_w^2 \epsilon^2 (c_2 - 16\pi c_\Lambda c_1) + m_h^2 (c_3 + 16\pi c_\Lambda c_4)]^2}{(4\pi)^7 c_Q^2 c_\Lambda^2 v_w^6} + \mathcal{O}(s_\theta^4, c_i^3). \quad (3.6)$$

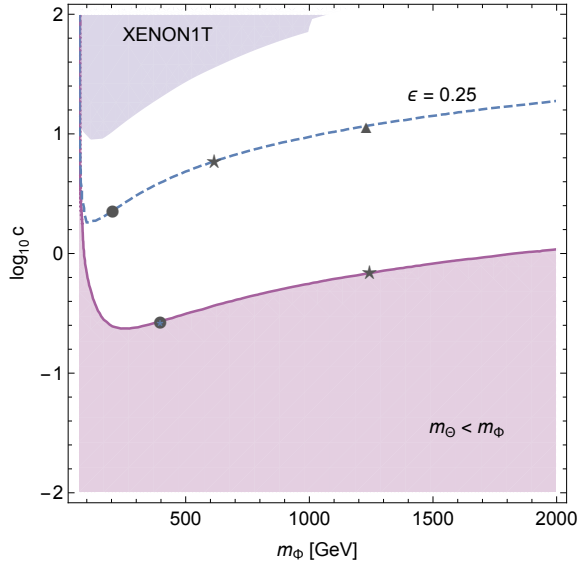


Figure 1: The thermal cross section in the CH case for $c_1 = c_2 = c_3 = c_4 \equiv c$ as a function of the DM mass, m_Φ . We fix the DM mass as a function of compositeness scale, f , via $m_\Phi = \epsilon f$ and let ϵ vary. The purple solid line corresponds to the thermal cross section $\langle \sigma v \rangle = 3 \cdot 10^{-26} \text{ cm}^3 \text{ s}^{-1}$ for $\epsilon = \max \epsilon(m_\Phi)$ for which $m_\Theta = m_\Phi$. We show $\max \epsilon(m_\Phi)$ in blue in Fig. 2. In the shaded region below the purple solid line, the relic density is too small due to the annihilation channel $\Phi\bar{\Phi} \rightarrow \Theta\Theta$ opening. The upper shaded region shows the XENON1T exclusion [62, 63] for $\epsilon = \max \epsilon(m_\Phi)$; for smaller ϵ , the region moves upwards, see Eq. (3.14). The dot, star, and triangle correspond to $s_\theta = 0.3, 0.1, 0.05$, respectively. Finally the blue dashed line shows the thermal cross section for a fixed $\epsilon = 0.25$.

The leading contribution from $\Phi\bar{\Phi} \rightarrow h \rightarrow \bar{t}t$ is $\mathcal{O}(s_\theta^4)$ and is given by

$$\langle \sigma v \rangle_{\bar{t}t} = \frac{3s_\theta^4 m_h^4 m_t^2 (c_3 + 16\pi c_\Lambda c_4)^2}{(4\pi)^7 c_Q^2 c_\Lambda^2 v_w^8} + \mathcal{O}(s_\theta^6). \quad (3.7)$$

The relative contributions of $\langle \sigma v \rangle_{\bar{t}t}$ and the two parts $\langle \sigma v \rangle_{hh,VV}^{1,2}$ and $\langle \sigma v \rangle_{hh,VV}^{3,4}$ from the $c_{1,2}$ and $c_{3,4}$ coefficients respectively are therefore

$$\frac{\langle \sigma v \rangle_{\bar{t}t}}{\langle \sigma v \rangle_{hh,VV}^{3,4}} = \frac{3s_\theta^2 m_t^2}{4\epsilon^2 v_w^2}, \quad \frac{\langle \sigma v \rangle_{hh,VV}^{3,4}}{\langle \sigma v \rangle_{hh,VV}^{1,2}} = \frac{1}{32\pi c_Q \epsilon^2} \frac{m_h^2 (c_3 + 16\pi c_\Lambda c_4)^2}{(c_2 - 16\pi c_\Lambda c_1)^2} \quad (3.8)$$

showing how the contact interactions, in particular the VV interactions from the $c_{1,2}$ terms, dominate the annihilation cross-section parametrically in s_θ . These contact interactions are however loop-suppressed in direct-detection scattering.

Values of $\epsilon \sim \mathcal{O}(1)$ will quite naturally lead to the right thermal relic density again with $s_\theta \lesssim 0.1$, while the requirement $m_\Theta > m_\Phi$ sets an upper bound $\epsilon \leq 1/2$.

Setting $c_1 = c_2 = c_3 = c_4 \equiv c$, and $c_\Lambda = 1$, we show the thermal cross section $\langle \sigma v \rangle = 3 \cdot 10^{-26} \text{ cm}^3 \text{ s}^{-1}$ as a function of c and m_Φ for different values of ϵ in Fig. 1. The blue dashed line corresponds to fixed value $\epsilon = 0.25$, whereas on the purple solid line, $\epsilon = \max \epsilon(m_\Phi)$ corresponding to the limit $m_\Theta = m_\Phi$. We show $\epsilon = \max \epsilon(m_\Phi)$ in Fig. 2. On the shaded purple region $m_\Theta < m_\Phi$, and the relic abundance would be washed away by the $\Phi\bar{\Phi} \rightarrow \Theta\Theta$ scatterings. The blue shaded region shows the current direct-detection

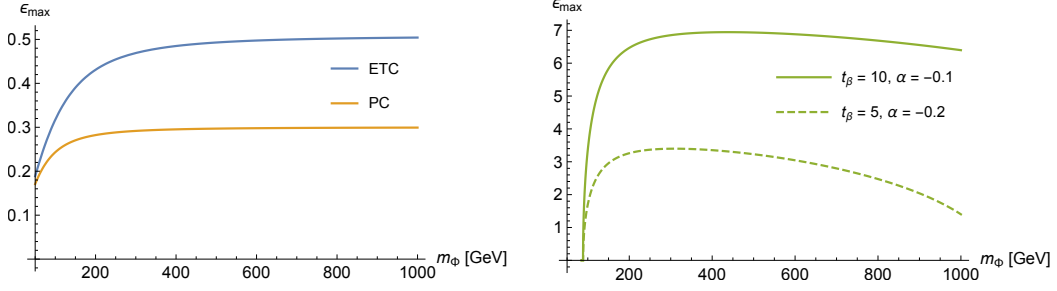


Figure 2: The maximal value of $\epsilon = m_\Phi/f$ corresponding to $m_\Theta = m_\Phi$ in ETC and fermion PC scenarios (left panel), and for the benchmark cases $t_\beta = 10, \alpha = -0.1, t_\beta = 5, \alpha = -0.2$, in the partially composite Higgs scenario (right panel) as a function of m_Φ .

limits by XENON1T [62, 63] assuming $\epsilon = \max \epsilon(m_\Phi)$. The direct-detection limits are discussed in more detail in Sec. 3.2.

(ii) Partially composite Higgs. Including an elementary Higgs doublet changes the picture significantly. Now CP-even states σ_h and h mix as described in Sec. 2.3, and the mass eigenstates are the physical Higgs boson, h_1 , and a heavy scalar, h_2 .

In this case, the thermal annihilation cross section is determined by the scattering channels $\Phi\bar{\Phi} \rightarrow h_i h_j, VV, t\bar{t}$, where $i = 1, 2$. In the simplified case, where the additional scalar is heavy, and only $\Phi\bar{\Phi} \rightarrow h_1 h_1, VV$ channels contribute, we can write the cross section as

$$\langle\sigma v\rangle = \frac{s_\theta^2 \epsilon^6 (16\pi c_\Lambda c_1 + c_2)^2 (s_\beta^4 + 3c_\beta^4)}{16\pi^5 c_\Lambda^2 c_\beta^2 v_w^2} - \frac{s_\theta^4 t_\beta^4 \epsilon^4 m_h^2 (16\pi c_\Lambda c_1 + c_2) (16\pi c_\Lambda c_4 - c_3)}{256\pi^6 c_\Lambda^2 c_Q c_\beta^2 v_w^4 \delta}, \quad (3.9)$$

and we again take $m_\Phi = \epsilon f$, but now $f_\Lambda = f = v_w c_\beta / s_\theta$. We fix m_Q and y_Q via the vacuum conditions, and trade m_H^2 and λ_H for δ (defined in Eq. (2.34)) and m_h^2 .

We show the full result including the additional scalar channels, while again setting $c_1 = c_2 = c_3 = c_4 \equiv c$ and $c_\Lambda = 1$, in Fig. 3 for two benchmark values of the additional angles: (a) $t_\beta = 10, \alpha = -0.1$ (left panel), and (b) $t_\beta = 5, \alpha = -0.2$ (right panel). Again, the solid purple curve represents the thermal cross section $\langle\sigma v\rangle = 3 \cdot 10^{-26} \text{ cm}^3 \text{ s}^{-1}$ for $\epsilon = \max \epsilon(m_\Phi)$ corresponding to the limit $m_\Theta = m_\Phi$ (see Fig. 2), and the dashed blue curve corresponds to a fixed $\epsilon = 1$. On the shaded purple region $m_\Theta < m_\Phi$, and upper shaded region shows the XENON1T exclusion [62, 63] for $\epsilon = \max \epsilon(m_\Phi)$. The associated heavy scalar spectrum corresponding to the benchmark cases (a) and (b) is shown in Fig. 4 as a function of s_θ . The kink in the thermal cross section lines are due to the opening of the $\Phi\bar{\Phi} \rightarrow h_1 h_2$ annihilation channel which yields the right relic abundance with lower values of c .

The top channel is now very subleading

$$\langle\sigma v\rangle_{t\bar{t}} = \frac{3s_\theta^8 s_\beta^8 m_h^4 m_t^2 s_{\alpha-\beta}^4 (c_3 - 16\pi c_\Lambda c_4)^2}{16\pi^7 s_{2\beta}^{10} c_Q^2 c_\Lambda^2 \delta^2 v_w^8} + \mathcal{O}(s_\theta^{10}). \quad (3.10)$$

(iii) Fermion partial compositeness. Taking $m_\Phi = \epsilon f$, and $f_\Lambda = f = v_w / s_\theta$, and m_Q fixed by the alignment condition Eq. (2.42), we find the corresponding cross

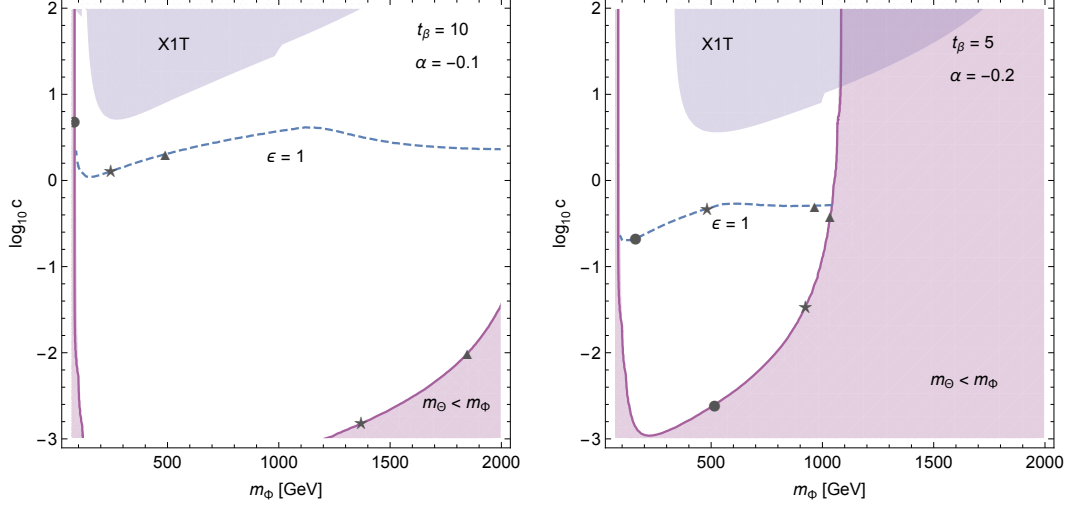


Figure 3: The thermal cross section in the pCH case with $c_1 = c_2 = c_3 = c_4 \equiv c$ as a function of the DM mass, $m_\Phi = \epsilon f$, for two benchmark cases: $t_\beta = 10, \alpha = -0.1$ (left panel) and $t_\beta = 5, \alpha = -0.2$ (right panel). The blue dashed line corresponds the thermal cross section $\langle\sigma v\rangle = 3 \cdot 10^{-26} \text{ cm}^3 \text{ s}^{-1}$ for fixed value $\epsilon = 1$, whereas on the purple solid line, $\epsilon = \max \epsilon(m_\Phi)$ corresponding to $m_\Theta = m_\Phi$; see Fig. 2. The upper shaded region shows the XENON1T exclusion [62, 63] assuming $\epsilon = \max \epsilon(m_\Phi)$; for smaller ϵ , the region moves upwards. The dot, star, and triangle correspond to $s_\theta = 0.3, 0.1, 0.05$, respectively.

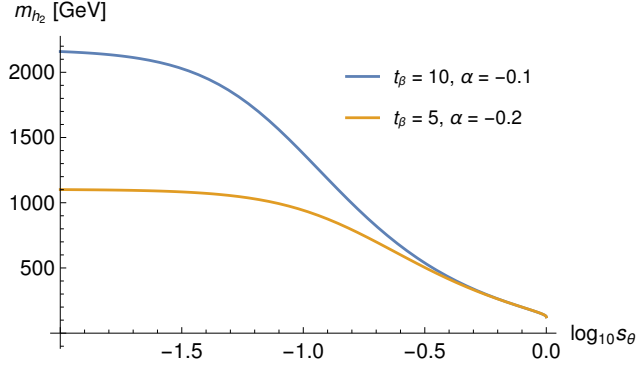


Figure 4: The mass of h_2 as a function of s_θ for the cases shown in Fig. 3. The masses of η and $\pi^{\pm,0}$ follow closely the mass of h_2 and we have omitted those for clarity.

section including $\Phi\bar{\Phi} \rightarrow hh, VV$ channels ($\eta\eta$ channel is again excluded by the $m_\Theta > m_\Phi$ condition):

$$\langle\sigma v\rangle = \frac{64s_\theta^2\epsilon^2}{(4\pi)^{11}c_\Lambda^2c_Q^2C_Y^4c_W^6} [C_{tS}(16\pi c_\Lambda c_4 + c_3)(8\pi^2 m_t^2 - C_{yS}^2 v_w^2 y_{tR}^4) - 128\pi^3 c_Q C_{yS}^2 v_w^2 \epsilon^2 (c_2 - 16\pi c_\Lambda c_1)]^2 + \mathcal{O}(s_\theta^4, c_i^3) \quad (3.11)$$

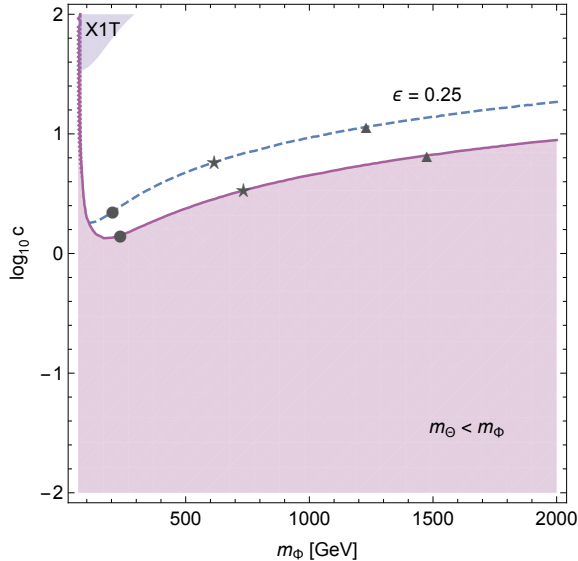


Figure 5: The thermal cross section in the PC case for $c_1 = c_2 = c_3 = c_4 \equiv c$ as a function of the DM mass, $m_\Phi = \epsilon f$. We have fixed $C_{yS} = 10, C_{tS} = 1$. The blue dashed line corresponds the thermal cross section $\langle\sigma v\rangle = 3 \cdot 10^{-26} \text{ cm}^3\text{s}^{-1}$ for fixed value $\epsilon = 0.25$, whereas on the purple solid line, $\epsilon = \max \epsilon(m_\Phi)$ corresponding to $m_\Theta = m_\Phi$; see Fig. 2. The upper shaded region shows the XENON1T exclusion [62, 63] assuming $\epsilon = \max \epsilon(m_\Phi)$. The dot, star, and triangle correspond to $s_\theta = 0.3, 0.1, 0.05$, respectively.

The leading contribution from $\Phi\bar{\Phi} \rightarrow t\bar{t}$ is $\mathcal{O}(s_\theta^4)$ and is given by

$$\langle\sigma v\rangle_{t\bar{t}} = \frac{48C_{tS}^2 m_t^2 s_\theta^4 (16\pi c_\Lambda c_4 + c_3)^2 \left(8\pi^2 m_t^2 - C_{yS}^2 v_w^2 y_{tR}^4\right)^2}{(4\pi)^{11} C_{yS}^4 c_Q^2 c_\Lambda^2 v_w^8} + \mathcal{O}(s_\theta^6). \quad (3.12)$$

We show again the thermal cross section for $c_1 = c_2 = c_3 = c_4 \equiv c$, $c_\Lambda = 1$, and $C_{yS} = 10, C_{tS} = 1$ as a function of c and m_Φ in Fig. 5. The blue dashed line corresponds to fixed value $\epsilon = 0.25$, and the purple solid line to $\epsilon = \max \epsilon(m_\Phi)$ for which $m_\Theta = m_\Phi$; see Fig. 2. We note that the χ sector is assumed to be heavy.

3.2 Experimental searches

The models we describe here can be experimentally searched for in multiple experiments including (i) via underground direct-detection experiments searching for signals of DM scattering off nuclei, (ii) via direct production of the DM particles and other composite states or deviations in SM measurements at the LHC experiments, or (iii) indirectly via satellite missions looking for signals of DM annihilating into SM particles in the gamma-ray spectrum from astrophysical objects with high DM density. We describe in this section the expectations for each of these types of searches.

(i) Direct detection. Since the contact interactions that determine the thermal relic density are loop suppressed in direct detection experiments, we expect the t -channel exchange of the (partially) composite scalars ($h_{1,2}$) h (Fig. 6(a)) will dominate the signal

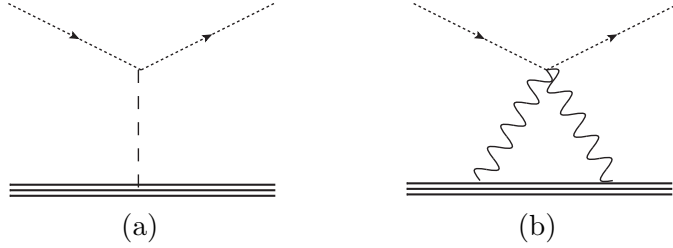


Figure 6: *Left:* Higgs exchange contribution to DD. *Right:* WW loop.

with a tree-level scattering cross-section on nuclei given by [64]:

$$\sigma_{\text{nucleon}}^H = \frac{\mu_N^2}{4\pi m_\Phi^2} \left[\frac{g_H d_H f_N m_N}{v_w} \right]^2, \quad (3.13)$$

where μ_N is the nucleon-DM reduced mass, m_N the nucleon mass, v_w the electroweak vev, g_H is the effective coupling between the DM and the relevant (partially) composite Higgs, $H = h, h_1, h_2$, d_H describes the scalar exchange, and f_N parametrizes the Higgs-nucleon coupling.

We take the central value of $f_N = 0.3$ [65, 66] but this value depends on whether all fermion masses arise from the same mechanism or if e.g. only the top quark fermion mass does. The effective coupling g_H is given in the limit of vanishing momentum transfer, $t \rightarrow 0$, by (cf. Eq. (2.15))

$$g_H = \frac{m_\Phi^2}{f_\Lambda^2} (g_h - g_{\partial h}) = \epsilon^2 (g_h - g_{\partial h}), \quad (3.14)$$

where in the last equality we have used our assumption $f_\Lambda = f$. Depending on the SM-fermion mass mechanism, d_H is given by

$$d_H^{\text{CH,PC}} = \frac{1}{m_h^2}, \quad (3.15)$$

$$d_H^{\text{pCH}} = \frac{s_\alpha c_\alpha}{s_\beta} \left(-\frac{1}{m_{h_1}^2} + \frac{1}{m_{h_2}^2} \right).$$

The direct detection cross-section from the contact interactions are loop suppressed and the dominant ones from W (Z) exchange are shown in Fig. 6(b). Loop-induced direct-detection constraints from four-particle contact interactions between DM and SM photons and vectors bosons were evaluated in e.g. Refs [67, 68] for interactions via field strength tensors and for inelastic transitions in Ref. [69]. Here however the interaction proceeds via the mass-like contact interaction, and we find the cross section

$$\sigma_{\text{nucleon}}^{VV} = \frac{1}{16\pi} \left(\frac{(c_2 - 16\pi c_1 c_\Lambda) g^2 g_{NV} m_N m_\Phi q}{64\sqrt{2}\pi^2 c_\Lambda f^2 f_\Lambda^2} \right)^2, \quad (3.16)$$

where g_{NV} ($V = Z, W$) parametrizes the vector boson-nucleon couplings. For $c_\Lambda = 1$, $q = 1$ GeV, we get

$$\sigma_{\text{nucleon}}^{VV} \approx (8.0g_{WN}^2 + 6.8g_{ZN}^2)(c_2 - 16\pi c_1)^2 s_\theta^6 \epsilon^2 10^{-53} \text{ cm}^2. \quad (3.17)$$

The resulting cross-section level is well below current direct-detection limits and below the neutrino floor. While in general there could be interference between the Higgs exchange and weak boson loop exchange, given how small the latter is, we do not consider that here. In summary, the annihilation cross section is dominated by the contact interactions of Φ with the SM vector bosons, while direct detection is dominated by the tree-level Higgs exchange.

(ii) The LHC experiments. The DM sector can be searched for at the LHC via missing energy signals. One class of such searches are the mono- X channels with missing energy where X is a jet, photon, a vector boson $V = Z, W$ or a Higgs boson [70–72]. The most distinct channels for our model are the $\bar{q}q$ initiated mono- V channels, $pp \rightarrow V^* \rightarrow V\Phi\bar{\Phi}$ through the quartic couplings in Eqs (A.1) and (A.2). The CMS and ATLAS experiments have looked at this kind of signature for a fermion DM candidate [73, 74] where dimension-5 operators are required. These searches have been interpreted for scalar DM with a $g_{\text{eff},V}V_\mu V^\mu\Phi\bar{\Phi}$ coupling in Ref. [75] but only to derive an order-of-magnitude bound for the effective couplings. Our case corresponds to a good approximation to

$$g_{\text{eff},Z} = \frac{m_\Phi^2}{f_\lambda^2}(d_{ZZ} + g_{ZZ}) = \epsilon^2(g'^2 + g^2)s_\theta^2 \left(\frac{c_2}{4\pi^2} + \frac{4c_1}{\pi} \right), \quad (3.18)$$

and currently only $g_{\text{eff},Z} \gg 1$ is excluded [75]. For instance, in the ETC case where the correct relic abundance can be obtained when $\epsilon \lesssim 0.5$ (see Fig. 2), $g_{\text{eff},Z} = 1$ corresponds to $c \sim 80$ assuming $c = c_1 = c_2$ and $s_\theta = 0.3$. Since the expression Eq. (3.18) has a similar dependence on θ and ϵ as the direct-detection bounds, even an optimistic bound on $g_{\text{eff},Z}$ is at best comparable to the X1T limits. However, the inclusion of spin-one resonances can produce distinct p_T spectra in these searches as shown in Ref. [76] and deserves to be investigated in detail. The monojet and monophoton limits on DM coupling to the SM via the Higgs portal, $pp \rightarrow HX \rightarrow \Phi\bar{\Phi}X$ are presented e.g. in Ref. [77]. Limits on the coupling $gvh\Phi\bar{\Phi}$ are $g \lesssim 1$ at $m_\Phi \simeq 100$ GeV and decrease at higher values of m_Φ , but our equivalent coupling is orders of magnitude smaller.

The new strong sector can also be searched for directly at the LHC and future colliders. Depending on parameters the LHC might be able to directly produce the pNGBs η and Θ of Table 2 together with the additional $h_2, \pi^{\pm,0}$ in the pCH scenario (see Eq. (2.33)) or the Θ_2 state in the PC scenario (see App. B).

A new aspect of our model, which has not yet been studied in detail, is the appearance of the light Θ boson, which is a mixture of an inert and an EW charged component. In addition, in the PC case we expect two further pNGBs as discussed above, which might lead to signatures not yet explored. Again they are here mixed with an inert sector and a careful analysis must be carried out. We leave this analysis for future work. We note that in the PC case, other (probably heavier) QCD charged pNGB are present, and their phenomenology has been studied in Ref. [78].

The phenomenology of η has been studied in Ref. [79] and the partially elementary scalars in Refs [15, 16]. Furthermore, in Ref. [59], it was shown that the η and η' corresponding to the quantum anomalous U(1) could be used to disentangle the three different fermion mass mechanisms we consider here. In Refs [58, 80], these bosonic states have been studied in a PC scenarios with both an EW sector and a QCD-colored sector but without inert fermions.

In summary, the model, and in particular its DM sector, leads to potentially rich collider phenomenology, but we leave the detailed study of it for future work.

(iii) Indirect detection. Finally the Fermi-LAT limits from DM annihilations in dwarf spheroidals [81] do not currently exclude a full thermal annihilation cross-section

into WW and ZZ at any mass. This is in contrast to direct detection which is seen to do so, e.g. in the right panel of Fig. 3. We therefore do not include indirect detection in our limit plots. However, we note that with a order of magnitude improvement in the experimental sensitivity, the DM mass range $m_W \lesssim m_\Phi \lesssim 500$ GeV can be probed.

4 Conclusions

In this paper we have constructed new (partially) composite Goldstone Higgs models featuring composite Goldstone DM candidates. The DM candidates are stabilized by U(1) global symmetries of the underlying four-dimensional gauge and gauge-Yukawa theories with strongly interacting fermions—analogueous to the U(1) baryon symmetry responsible for the longevity of the proton. However, differently from the proton, the thermal relic density of the DM is particle anti-particle symmetric.

Only part of the strongly interacting fermions are gauged under the EW symmetry of the SM and the DM particle is the lightest particle charged under the global U(1) among the SM-inert fermions. At the effective Lagrangian level the DM relic density arises from double trace terms between the SM-inert-sector fermions and those that are gauged under the SM symmetry group. In particular these double trace terms provide four-point contact-interaction terms between the DM and the SM vector bosons—as well as the Higgs and additional pNGBs—which determine the thermal relic density.

The dominant scattering channel for direct detection is via composite Higgs exchange arising also from double trace terms. The Higgs couplings to the DM particle is sensitive to the origin of the SM fermion masses, either via ETC-type four-fermion operators, mixing with elementary doublets, or via fermion partial compositeness. Therefore direct detection is in principle able to probe this origin; however, the constraints are overall weak and only exclude regions with unexpectedly large values of the Gasser–Leutwyler type coefficients in the effective Lagrangian.

We eliminate the annihilation channel of the DM, Φ , into the additional pNGB, Θ , related to the global U(1) factor by requiring that $m_\Theta > m_\Phi$. This is the only annihilation channel that arises at single-trace level and which could wash out the thermal relic density. This requirement selects vacuum angles in the region $\sin \theta \sim 0.01 - 1$ again depending on the fermion mass mechanism and assuming that the effective Lagrangian coefficients, c_i , are $\mathcal{O}(1)$ as expected by naive dimensional analysis. Therefore, the requirement eliminates the fine-tuned decoupling limit of parameter space where $\sin \theta \ll 1$.

The SM inert fermions may render the strong dynamics near-conformal and this may imply that the composite spin-one spectrum exhibits nearly parity doubling. In the TC limit this has been argued to reduce the electroweak S parameter. Although in CH models with a large compositeness scale, f , such a dynamical reduction is not necessary to be in agreement with experimental constraints, it would be interesting to explore in partially composite Higgs models where the scale f can be low. The presence of an explicit underlying model with composite Higgs and DM opens the possibility for the lattice to provide crucial input to the phenomenology of these models such as a precise determination of the spectrum.

Finally, the unique features of the model might present yet unexplored signatures at the LHC and future colliders.

Acknowledgments

MTF and MJ acknowledges partial funding from The Council For Independent Research, grant number DFF 6108-00623. The CP3-Origins centre is partially funded by the Danish National Research Foundation, grant number DNRF90. DBF acknowledges partial funding

by the European Union as a part of the H2020 Marie Skłodowska-Curie Initial Training Network MCnetITN3 (722104).

A Φ -interactions

Here we give explicitly the couplings in Eq. (2.15),

$$\begin{aligned}
\mathcal{L}_{Q,\Lambda} \supset & \frac{m_\Phi^2}{f_\Lambda^2} \Phi \bar{\Phi} \left(g_{hh} h + \frac{1}{2} g_{ZZ} Z_\mu Z^\mu + g_{WW} W_\mu^+ W^{-\mu} + \frac{1}{2} g_{\Theta\Theta} \Theta^2 + \frac{1}{2} g_{hh} h^2 + \frac{1}{2} g_{\eta\eta} \eta^2 \right. \\
& \left. + \frac{1}{2} g_{\partial\Theta} \partial_\mu \Theta \partial^\mu \Theta + \frac{1}{2} g_{\partial h} \partial_\mu h \partial^\mu h + \frac{1}{2} g_{\partial\eta} \partial_\mu \eta \partial^\mu \eta \right) \\
& + \frac{1}{f_\Lambda^2} \partial_\mu \Phi \partial^\mu \bar{\Phi} \left(d_h h + \frac{1}{2} d_{ZZ} Z_\mu Z^\mu + d_{WW} W_\mu^+ W^{-\mu} + \frac{1}{2} d_{hh} h^2 + \frac{1}{2} d_{\eta\eta} \eta^2 \right. \\
& \left. + \frac{1}{2} d_{\partial\Theta} \partial_\mu \Theta \partial^\mu \Theta + \frac{1}{2} d_{\partial h} \partial_\mu h \partial^\mu h + \frac{1}{2} d_{\partial\eta} \partial_\mu \eta \partial^\mu \eta \right). \tag{A.1}
\end{aligned}$$

These read

$$\begin{aligned}
g_h &= \frac{c_3 m_Q s_\theta}{2 c_\Lambda \pi^2}, & d_h &= \frac{8 c_4 m_Q s_\theta}{\pi}, \\
g_{ZZ} &= -\frac{(g_L^2 + g_Y^2) c_2 s_\theta^2}{4 \pi^2 c_\Lambda}, & d_{ZZ} &= \frac{4(g_L^2 + g_Y^2) c_1 s_\theta^2}{\pi}, \\
g_{WW} &= -\frac{c_2 g_L^2 s_\theta^2}{4 \pi^2 c_\Lambda}, & d_{WW} &= \frac{4 g_L^2 c_1 s_\theta^2}{\pi}, \\
g_{\Theta\Theta} &= \frac{8 \pi^2 c_\Lambda f_\Lambda^2 + 4 c_3 m_Q f c_\theta}{9 \pi^2 c_\Lambda f_\Theta^2}, & d_{\Theta\Theta} &= \frac{64 c_4 m_Q f c_\theta}{9 \pi f_\Theta^2}, \\
g_{\partial\Theta} &= -\frac{8 c_2}{9 \pi^2 c_\Lambda f_\Theta^2}, & d_{\partial\Theta} &= \frac{128 c_1}{9 \pi f_\Theta^2}, \\
g_{hh} &= \frac{c_3 m_Q c_\theta}{2 \pi^2 c_\Lambda f}, & d_{hh} &= \frac{8 c_4 m_Q c_\theta}{\pi f}, \\
g_{\partial h} &= -\frac{c_2}{\pi^2 c_\Lambda f^2}, & d_{\partial h} &= \frac{16 c_1}{\pi f^2}, \\
g_{\eta\eta} &= \frac{c_3 m_Q c_\theta}{2 \pi^2 c_\Lambda f}, & d_{\eta\eta} &= \frac{8 c_4 m_Q c_\theta}{\pi f}, \\
g_{\partial\eta} &= -\frac{c_2}{\pi^2 c_\Lambda f^2}, & d_{\partial\eta} &= \frac{16 c_1}{\pi f^2}
\end{aligned} \tag{A.2}$$

B Abelian bosons

In a general underlying theory with n fermionic sectors, each one specified by a representation r and a number of fermions N_r , there is a global symmetry $U(1)^n$ one of which is anomalous under G_{TC} and the anomaly-free combinations are given by

$$\sum_r q_r T(r) = 0, \tag{B.1}$$

where $T(r)$ is the index of the representation r . Each $U(1)$ can be associated with a boson Θ_r and $n - 1$ of them are pNGBs. The masses of these states can be parametrized by

$$V_m = \sum_r \frac{1}{2} m_r^2 \Theta_r^2 + \frac{1}{2} m_A^2 \Theta'^2, \tag{B.2}$$

where m_A is the mass generated by the anomaly and Θ' is the corresponding state. The states Θ_r can be parametrized inside the NGB matrices of Eq. (2.7) in the following way

$$\Sigma_r = \exp \left[2\sqrt{2}i \left(\frac{\Pi_r}{f_r} + \frac{\Theta_r}{\sqrt{2N_r}f_{\Theta_r}} \mathbb{1}_{N_r} \right) \right] E_r, \quad (\text{B.3})$$

which defines canonically normalised kinetic terms from Eq. (2.10). $\mathbb{1}_{N_r}$ is the identity matrix of dimension N_r . We proceed defining $n-1$ anomaly-free states Θ_i ($i = 1, \dots, n-1$) and the anomalous $\Theta' \equiv \Theta_n$, with

$$\Theta_r = \sqrt{2N_r}f_r \left(\sum_i q_{r,i} \frac{\Theta_i}{\mathcal{N}_i} \right), \quad \mathcal{N}_i = \sum_r \sqrt{2N_r}f_r q_{r,i}. \quad (\text{B.4})$$

The factor \mathcal{N}_i guarantees a proper normalization of the fields and

$$\sum_i q_{r,i} q_{r',i} = 0 \quad (\text{B.5})$$

guarantees no kinetic mixing. The charges of Θ_n that defines the anomalous combination are given by the vector perpendicular to the plane defined by the indexes,

$$q_{r,n} = T(r). \quad (\text{B.6})$$

The other charges are then defined to span the rest of the space with orthogonal basis. These states then mass mix via the terms in Eq. (B.2) to form physical states.

In ETC and pCH cases we assumed $n = 2$ fermion representations, \mathbf{Q} in \mathbf{F} and λ in \mathbf{G} of $G_{\text{TC}} = \text{SU}(2)$, which give rise to 2 external $\text{U}(1)$ groups one of which is anomalous. The anomalous charges are $q_{F,2} = 1/2$ and $q_{G,2} = 2$ and the anomaly-free one is the orthogonal combination $q_{G,1} = 1/2$ and $q_{F,1} = -1$. They mix according to Eq. (B.2) and in the Θ' decoupled limit ($m_A \rightarrow \infty$) we recover Eq. (3.15): $m_{\Theta}^2 = \frac{1}{9}(8m_F^2 + m_G^2)$ with $m_F = m_\eta c_\theta$ and $m_G = m_\Phi$. A similar situation with two sectors has been studied in Ref. [58].

In PC case we assumed a $n = 3$ fermionic sectors, \mathbf{Q} in \mathbf{F} , λ in \mathbf{G} and χ in \mathbf{A}_2 of $G_{\text{TC}} = \text{Sp}(4)$. The anomalous combination is $q_{F,3} = 1$, $q_{A_2,3} = 3$, $q_{G,3} = 3$. In the case the anomalous field is decoupled we have the masses of the two anomaly-free states given by

$$m_{\Theta_1, \Theta_2}^2 = \frac{1}{152} \left\{ 23m_\Phi^2 + 72m_F^2 + 52m_\chi^2 \pm [5184m_F^4 - 432m_F^2(5m_\Phi^2 + 19m_\chi^2) + 529m_\Phi^4 + 1710m_\Phi^2m_\chi^2 + 3249m_\chi^4]^{1/2} \right\} \quad (\text{B.7})$$

with $m_F = m_\eta c_\theta$. If the χ sector decouples ($m_\chi \rightarrow \infty$) then we recover the expression in Eq. (2.47): $m_{\Theta}^2 = \frac{1}{19}(18m_\eta^2 c_\theta^2 + m_\Phi^2)$. If $m_\chi \ll m_F$ then $m_{\Theta_1}^2 \approx \frac{1}{4}(m_\Phi^2 + 3m_\chi^2)$ and the phenomenology changes. This situation was not considered here and we leave it for future analysis.

References

- [1] E. Eichten and K. D. Lane, *Dynamical Breaking of Weak Interaction Symmetries*, *Phys. Lett.* **B90** (1980) 125–130.
- [2] S. Dimopoulos and L. Susskind, *Mass Without Scalars*, *Nucl. Phys.* **B155** (1979) 237–252.
- [3] F. Sannino and K. Tuominen, *Orientifold theory dynamics and symmetry breaking*, *Phys.Rev.* **D71** (2005) 051901, [[hep-ph/0405209](#)].

- [4] D. D. Dietrich, F. Sannino, and K. Tuominen, *Light composite Higgs from higher representations versus electroweak precision measurements: Predictions for CERN LHC*, *Phys. Rev.* **D72** (2005) 055001, [[hep-ph/0505059](#)].
- [5] R. Foadi, M. T. Frandsen, and F. Sannino, *125 GeV Higgs from a not so light Technicolor Scalar*, *Phys.Rev.* **D87** (2013) 095001, [[arXiv:1211.1083](#)].
- [6] G. 't Hooft, *Naturalness, chiral symmetry, and spontaneous chiral symmetry breaking*, *NATO Sci. Ser. B* **59** (1980) 135.
- [7] E. H. Simmons, *Phenomenology of a Technicolor Model With Heavy Scalar Doublet*, *Nucl.Phys.* **B312** (1989) 253.
- [8] S. Samuel, *BOSONIC TECHNICOLOR*, *Nucl. Phys.* **B347** (1990) 625–650.
- [9] A. Kagan and S. Samuel, *The Family mass hierarchy problem in bosonic technicolor*, *Phys. Lett.* **B252** (1990) 605–610.
- [10] C. D. Carone, *Technicolor with a 125 GeV Higgs Boson*, *Phys.Rev.* **D86** (2012) 055011, [[arXiv:1206.4324](#)].
- [11] T. Alanne, S. Di Chiara, and K. Tuominen, *LHC Data and Aspects of New Physics*, *JHEP* **01** (2014) 041, [[arXiv:1303.3615](#)].
- [12] D. B. Kaplan and H. Georgi, *$SU(2) \times U(1)$ Breaking by Vacuum Misalignment*, *Phys.Lett.* **B136** (1984) 183.
- [13] J. Galloway, A. L. Kagan, and A. Martin, *A UV complete partially composite-pNGB Higgs*, *Phys. Rev.* **D95** (2017), no. 3 035038, [[arXiv:1609.05883](#)].
- [14] A. Agugliaro, O. Antipin, D. Becciolini, S. De Curtis, and M. Redi, *UV complete composite Higgs models*, *Phys. Rev.* **D95** (2017), no. 3 035019, [[arXiv:1609.07122](#)].
- [15] T. Alanne, D. Buarque Franzosi, and M. T. Frandsen, *A partially composite Goldstone Higgs*, *Phys. Rev.* **D96** (2017) 095012, [[arXiv:1709.10473](#)].
- [16] T. Alanne, D. Buarque Franzosi, M. T. Frandsen, M. L. A. Kristensen, A. Meroni, and M. Rosenlyst, *Partially composite Higgs models: Phenomenology and RG analysis*, *JHEP* **01** (2018) 051, [[arXiv:1711.10410](#)].
- [17] D. B. Kaplan, H. Georgi, and S. Dimopoulos, *Composite Higgs Scalars*, *Phys.Lett.* **B136** (1984) 187.
- [18] M. A. Luty and T. Okui, *Conformal technicolor*, *JHEP* **09** (2006) 070, [[hep-ph/0409274](#)].
- [19] G. Ferretti and D. Karateev, *Fermionic UV completions of Composite Higgs models*, *JHEP* **03** (2014) 077, [[arXiv:1312.5330](#)].
- [20] G. Ferretti, *UV Completions of Partial Compositeness: The Case for a $SU(4)$ Gauge Group*, *JHEP* **06** (2014) 142, [[arXiv:1404.7137](#)].
- [21] G. Cacciapaglia and F. Sannino, *Fundamental Composite (Goldstone) Higgs Dynamics*, *JHEP* **04** (2014) 111, [[arXiv:1402.0233](#)].
- [22] A. Belyaev, M. S. Brown, R. Foadi, and M. T. Frandsen, *The Technicolor Higgs in the Light of LHC Data*, [arXiv:1309.2097](#).
- [23] S. Nussinov, *TECHNOCOSMOLOGY: COULD A TECHNIBARYON EXCESS PROVIDE A 'NATURAL' MISSING MASS CANDIDATE?*, *Phys. Lett.* **165B** (1985) 55–58.
- [24] S. M. Barr, R. S. Chivukula, and E. Farhi, *Electroweak Fermion Number Violation and the Production of Stable Particles in the Early Universe*, *Phys. Lett.* **B241** (1990) 387–391.
- [25] S. B. Gudnason, C. Kouvaris, and F. Sannino, *Dark Matter from new Technicolor Theories*, *Phys. Rev.* **D74** (2006) 095008, [[hep-ph/0608055](#)].
- [26] T. A. Ryttov and F. Sannino, *Ultra Minimal Technicolor and its Dark Matter TIMP*, *Phys.Rev.* **D78** (2008) 115010, [[arXiv:0809.0713](#)].
- [27] M. T. Frandsen and F. Sannino, *iTIMP: isotriplet Technicolor Interacting Massive Particle as Dark Matter*, *Phys. Rev.* **D81** (2010) 097704, [[arXiv:0911.1570](#)].

- [28] M. T. Frandsen, S. Sarkar, and K. Schmidt-Hoberg, *Light asymmetric dark matter from new strong dynamics*, *Phys. Rev.* **D84** (2011) 051703, [[arXiv:1103.4350](#)].
- [29] A. Belyaev, M. T. Frandsen, S. Sarkar, and F. Sannino, *Mixed dark matter from technicolor*, *Phys. Rev.* **D83** (2011) 015007, [[arXiv:1007.4839](#)].
- [30] H. Ishida, S. Matsuzaki, and Y. Yamaguchi, *Bosonic-Seesaw Portal Dark Matter*, *PTEP* **2017** (2017), no. 10 103B01, [[arXiv:1610.07137](#)].
- [31] M. Frigerio, A. Pomarol, F. Riva, and A. Urbano, *Composite Scalar Dark Matter*, *JHEP* **07** (2012) 015, [[arXiv:1204.2808](#)].
- [32] A. Carmona and M. Chala, *Composite Dark Sectors*, *JHEP* **06** (2015) 105, [[arXiv:1504.00332](#)].
- [33] N. Fonseca, R. Zukanovich Funchal, A. Lessa, and L. Lopez-Honorez, *Dark Matter Constraints on Composite Higgs Models*, *JHEP* **06** (2015) 154, [[arXiv:1501.05957](#)].
- [34] G. Ballesteros, A. Carmona, and M. Chala, *Exceptional Composite Dark Matter*, *Eur. Phys. J.* **C77** (2017), no. 7 468, [[arXiv:1704.07388](#)].
- [35] Y. Wu, T. Ma, B. Zhang, and G. Cacciapaglia, *Composite Dark Matter and Higgs*, *JHEP* **11** (2017) 058, [[arXiv:1703.06903](#)].
- [36] T. Ma and G. Cacciapaglia, *Fundamental Composite 2HDM: $SU(N)$ with 4 flavours*, *JHEP* **03** (2016) 211, [[arXiv:1508.07014](#)].
- [37] C. Cai, G. Cacciapaglia, and H.-H. Zhang, *Vacuum alignment in a composite 2HDM*, [[arXiv:1805.07619](#)].
- [38] R. Balkin, M. Ruhdorfer, E. Salvioni, and A. Weiler, *Charged Composite Scalar Dark Matter*, *JHEP* **11** (2017) 094, [[arXiv:1707.07685](#)].
- [39] F. Sannino, A. Strumia, A. Tesi, and E. Vigiani, *Fundamental partial compositeness*, *JHEP* **11** (2016) 029, [[arXiv:1607.01659](#)].
- [40] D. D. Dietrich and F. Sannino, *Conformal window of $SU(N)$ gauge theories with fermions in higher dimensional representations*, *Phys. Rev.* **D75** (2007) 085018, [[hep-ph/0611341](#)].
- [41] M. A. Luty, *Strong Conformal Dynamics at the LHC and on the Lattice*, *JHEP* **04** (2009) 050, [[arXiv:0806.1235](#)].
- [42] J. Galloway, M. A. Luty, Y. Tsai, and Y. Zhao, *Induced Electroweak Symmetry Breaking and Supersymmetric Naturalness*, *Phys.Rev.* **D89** (2014) 075003, [[arXiv:1306.6354](#)].
- [43] R. Arthur, V. Drach, M. Hansen, A. Hietanen, C. Pica, and F. Sannino, *$SU(2)$ gauge theory with two fundamental flavors: A minimal template for model building*, *Phys. Rev.* **D94** (2016), no. 9 094507, [[arXiv:1602.06559](#)].
- [44] R. Arthur, V. Drach, A. Hietanen, C. Pica, and F. Sannino, *$SU(2)$ Gauge Theory with Two Fundamental Flavours: Scalar and Pseudoscalar Spectrum*, [[arXiv:1607.06654](#)].
- [45] C. Pica, V. Drach, M. Hansen, and F. Sannino, *Composite Higgs Dynamics on the Lattice*, *EPJ Web Conf.* **137** (2017) 10005, [[arXiv:1612.09336](#)].
- [46] T. A. DeGrand, D. Hackett, W. I. Jay, E. T. Neil, Y. Shamir, and B. Svetitsky, *Towards Partial Compositeness on the Lattice: Baryons with Fermions in Multiple Representations*, *PoS LATTICE2016* (2016) 219, [[arXiv:1610.06465](#)].
- [47] V. Ayyar, T. DeGrand, D. C. Hackett, W. I. Jay, E. T. Neil, Y. Shamir, and B. Svetitsky, *Baryon spectrum of $SU(4)$ composite Higgs theory with two distinct fermion representations*, *Phys. Rev.* **D97** (2018), no. 11 114505, [[arXiv:1801.05809](#)].
- [48] R. Lewis, C. Pica, and F. Sannino, *Light Asymmetric Dark Matter on the Lattice: $SU(2)$ Technicolor with Two Fundamental Flavours*, *Phys. Rev.* **D85** (2012) 014504, [[arXiv:1109.3513](#)].
- [49] A. Hietanen, C. Pica, F. Sannino, and U. I. Sondergaard, *Orthogonal Technicolor with Isotriplet Dark Matter on the Lattice*, *Phys.Rev.* **D87** (2013), no. 3 034508, [[arXiv:1211.5021](#)].

- [50] A. Hietanen, R. Lewis, C. Pica, and F. Sannino, *Composite Goldstone Dark Matter: Experimental Predictions from the Lattice*, *JHEP* **12** (2014) 130, [[arXiv:1308.4130](#)].
- [51] **Lattice Strong Dynamics (LSD) Collaboration**, T. Appelquist et al., *Composite bosonic baryon dark matter on the lattice: $SU(4)$ baryon spectrum and the effective Higgs interaction*, *Phys. Rev.* **D89** (2014), no. 9 094508, [[arXiv:1402.6656](#)].
- [52] D. B. Kaplan, *Flavor at SSC energies: A New mechanism for dynamically generated fermion masses*, *Nucl. Phys.* **B365** (1991) 259–278.
- [53] D. Buarque Franzosi, G. Cacciapaglia, H. Cai, A. Deandrea, and M. Frandsen, *Vector and Axial-vector resonances in composite models of the Higgs boson*, *JHEP* **11** (2016) 076, [[arXiv:1605.01363](#)].
- [54] J. Galloway, J. A. Evans, M. A. Luty, and R. A. Tacchi, *Minimal Conformal Technicolor and Precision Electroweak Tests*, *JHEP* **1010** (2010) 086, [[arXiv:1001.1361](#)].
- [55] J. Gasser and H. Leutwyler, *Chiral Perturbation Theory: Expansions in the Mass of the Strange Quark*, *Nucl. Phys.* **B250** (1985) 465–516.
- [56] A. Manohar and H. Georgi, *Chiral Quarks and the Nonrelativistic Quark Model*, *Nucl. Phys.* **B234** (1984) 189–212.
- [57] M. Gell-Mann, R. J. Oakes, and B. Renner, *Behavior of current divergences under $SU(3) \times SU(3)$* , *Phys. Rev.* **175** (1968) 2195–2199.
- [58] A. Belyaev, G. Cacciapaglia, H. Cai, G. Ferretti, T. Flacke, A. Parolini, and H. Serodio, *Di-boson signatures as Standard Candles for Partial Compositeness*, *JHEP* **01** (2017) 094, [[arXiv:1610.06591](#)]. [Erratum: *JHEP*12,088(2017)].
- [59] T. Alanne, M. T. Frandsen, and D. Buarque Franzosi, *Testing a dynamical origin of Standard Model fermion masses*, *Phys. Rev.* **D94** (2016) 071703, [[arXiv:1607.01440](#)].
- [60] T. Alanne, N. Bizot, G. Cacciapaglia, and F. Sannino, *Classification of NLO operators for composite Higgs models*, *Phys. Rev.* **D97** (2018), no. 7 075028, [[arXiv:1801.05444](#)].
- [61] J. Barnard, T. Gherghetta, and T. S. Ray, *UV descriptions of composite Higgs models without elementary scalars*, *JHEP* **02** (2014) 002, [[arXiv:1311.6562](#)].
- [62] **XENON Collaboration**, E. Aprile et al., *First Dark Matter Search Results from the XENON1T Experiment*, *Phys. Rev. Lett.* **119** (2017), no. 18 181301, [[arXiv:1705.06655](#)].
- [63] **XENON Collaboration**, E. Aprile et al., *Dark Matter Search Results from a One Tonne \times Year Exposure of XENON1T*, [[arXiv:1805.12562](#)].
- [64] J. McDonald, *Gauge singlet scalars as cold dark matter*, *Phys. Rev.* **D50** (1994) 3637–3649, [[hep-ph/0702143](#)].
- [65] J. M. Alarcon, J. Martin Camalich, and J. A. Oller, *The chiral representation of the πN scattering amplitude and the pion-nucleon sigma term*, *Phys. Rev.* **D85** (2012) 051503, [[arXiv:1110.3797](#)].
- [66] J. M. Alarcon, L. S. Geng, J. Martin Camalich, and J. A. Oller, *The strangeness content of the nucleon from effective field theory and phenomenology*, *Phys. Lett.* **B730** (2014) 342–346, [[arXiv:1209.2870](#)].
- [67] M. T. Frandsen, U. Haisch, F. Kahlhoefer, P. Mertsch, and K. Schmidt-Hoberg, *Loop-induced dark matter direct detection signals from gamma-ray lines*, *JCAP* **1210** (2012) 033, [[arXiv:1207.3971](#)].
- [68] A. Crivellin and U. Haisch, *Dark matter direct detection constraints from gauge bosons loops*, *Phys. Rev.* **D90** (2014) 115011, [[arXiv:1408.5046](#)].
- [69] M. Cirelli, N. Fornengo, and A. Strumia, *Minimal dark matter*, *Nucl. Phys.* **B753** (2006) 178–194, [[hep-ph/0512090](#)].
- [70] A. Birkedal, K. Matchev, and M. Perelstein, *Dark matter at colliders: A Model independent approach*, *Phys. Rev.* **D70** (2004) 077701, [[hep-ph/0403004](#)].

- [71] J. Goodman, M. Ibe, A. Rajaraman, W. Shepherd, T. M. P. Tait, and H.-B. Yu, *Constraints on Light Majorana dark Matter from Colliders*, *Phys. Lett.* **B695** (2011) 185–188, [[arXiv:1005.1286](#)].
- [72] P. J. Fox, R. Harnik, J. Kopp, and Y. Tsai, *Missing Energy Signatures of Dark Matter at the LHC*, *Phys. Rev.* **D85** (2012) 056011, [[arXiv:1109.4398](#)].
- [73] CMS Collaboration, A. M. Sirunyan et al., *Search for dark matter and unparticles in events with a Z boson and missing transverse momentum in proton-proton collisions at $\sqrt{s} = 13$ TeV*, *JHEP* **03** (2017) 061, [[arXiv:1701.02042](#)]. [Erratum: JHEP09,106(2017)].
- [74] ATLAS Collaboration, G. Aad et al., *Search for dark matter in events with a Z boson and missing transverse momentum in pp collisions at $\sqrt{s}=8$ TeV with the ATLAS detector*, *Phys. Rev.* **D90** (2014), no. 1 012004, [[arXiv:1404.0051](#)].
- [75] I. Brivio, M. B. Gavela, L. Merlo, K. Mimasu, J. M. No, R. del Rey, and V. Sanz, *Non-linear Higgs portal to Dark Matter*, *JHEP* **04** (2016) 141, [[arXiv:1511.01099](#)].
- [76] R. Foadi, M. T. Frandsen, and F. Sannino, *Technicolor Dark Matter*, *Phys. Rev.* **D80** (2009) 037702, [[arXiv:0812.3406](#)].
- [77] J. Ellis, A. Fowlie, L. Marzola, and M. Raidal, *Statistical Analyses of Higgs- and Z-Portal Dark Matter Models*, *Phys. Rev.* **D97** (2018), no. 11 115014, [[arXiv:1711.09912](#)].
- [78] G. Cacciapaglia, H. Cai, A. Deandrea, T. Flacke, S. J. Lee, and A. Parolini, *Composite scalars at the LHC: the Higgs, the Sextet and the Octet*, *JHEP* **11** (2015) 201, [[arXiv:1507.02283](#)].
- [79] A. Arbey, G. Cacciapaglia, H. Cai, A. Deandrea, S. Le Corre, and F. Sannino, *Fundamental Composite Electroweak Dynamics: Status at the LHC*, *Phys. Rev.* **D95** (2017), no. 1 015028, [[arXiv:1502.04718](#)].
- [80] G. Cacciapaglia, G. Ferretti, T. Flacke, and H. Serodio, *Revealing timid pseudo-scalars with taus at the LHC*, *Eur. Phys. J.* **C78** (2018), no. 9 724, [[arXiv:1710.11142](#)].
- [81] Fermi-LAT Collaboration, M. Ackermann et al., *Searching for Dark Matter Annihilation from Milky Way Dwarf Spheroidal Galaxies with Six Years of Fermi Large Area Telescope Data*, *Phys. Rev. Lett.* **115** (2015), no. 23 231301, [[arXiv:1503.02641](#)].